SANDIA REPORT

SAND2016-9773
Unlimited Release
September 2016

Controls on Incomplete Mixing of Injected Raw Water and Brine in Strategic Petroleum Reserve Salt Caverns

Jason E. Heath, Martin B. Nemer, and Kirsten N. Chojnicki

Prepared by
Sandia National Laboratories
Albuquerque, New Mexico 87185 and Livermore, California 94550

Sandia National Laboratories is a multi-mission laboratory managed and operated by Sandia Corporation, a wholly owned subsidiary of Lockheed Martin Corporation, for the U.S. Department of Energy's National Nuclear Security Administration under contract DE-AC04-94AL85000.

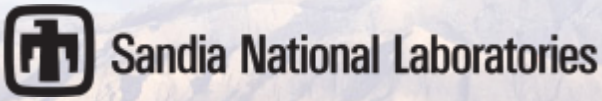

Issued by Sandia National Laboratories, operated for the United States Department of Energy by Sandia Corporation.

Available to DOE and DOE contractors from
U.S. Department of Energy
Office of Scientific and Technical Information
P.O. Box 62
Oak Ridge, TN 37831

Telephone: (865) 576-8401
Facsimile: (865) 576-5728
E-Mail: reports@osti.gov
Online ordering: http://www.osti.gov/scitech

Available to the public from
U.S. Department of Commerce
National Technical Information Service
5301 Shawnee Rd
Alexandria, VA 22312

Telephone: (800) 553-6847
Facsimile: (703) 605-6900
E-Mail: orders@ntis.gov
Online order: http://www.ntis.gov/search

SAND2016-9773
Unlimited Release
September 2016

Controls on Incomplete Mixing of Injected Raw Water and Brine in Strategic Petroleum Reserve Salt Caverns

Jason E. Heath
Geomechanics Department

Martin B. Nemer
Thermal Fluid Experimental Science Department

Kirsten N. Chojnicki
Geomechanics Department

Sandia National Laboratories
P.O. Box 5800, Mail Stop 0750
Albuquerque, New Mexico 87185-MS0750

Abstract

Mixing of injected raw (undersaturated) water with brine in Strategic Petroleum Reserve (SPR) salt caverns affects the shape of cavern walls due to leaching. Cavern shape impacts cavern geomechanical stability and available volume for oil storage. Raw water injection occurs during initial solution mining of caverns, remedial leaching of caverns, and oil drawdown. Of interest are factors that control the degree of raw water-brine mixing and thereby the concentration of the aqueous fluid mixture that contacts the salt cavern walls. It is hypothesized that poorly-mixed fresh water could potentially cause undesirable and non-uniform leaching, for example, if buoyant poorly-mixed fresh water collects and preferentially leaches under the oil-brine interface. This report presents current understanding of controls on incomplete-to-complete mixing of raw water and brine, focusing on implications for SPR cavern leaching. In the context of mixing, we review the following: SPR leaching operations; models of leaching; field measurements of leaching and cavern shapes; and previous laboratory experiments of mixing and/or leaching performed at Sandia National Laboratories. We present recent laboratory experiments in 2014-2016 that focused explicitly on understanding controls of poor-to-well mixed conditions. We find that well-mixed conditions are expected for typical operating conditions of the SPR.

CONTENTS

FIGURES

TABLES

NOMENCLATURE

ABI	Air-brine interface
bbl	Barrel (unit)
Fr	Froude number
OBI	Oil-brine interface
Re	Reynolds number
SNL	Sandia National Laboratories
SANSMIC	Sandia Solution-Mining Code
SPR	Strategic Petroleum Reserve
US DOE	United States Department of Energy

1. EXECUTIVE SUMMARY

This report reviews current understanding on the conditions that may lead from complete-to-incomplete mixing between injected raw water and brine in salt caverns of the Strategic Petroleum Reservoir (SPR). It has been hypothesized that incomplete mixing could lead to stratification of fresh water and brine, thereby enhancing local leaching of salt cavern walls. Localized leaching could cause irregularly shaped caverns and lead to mechanical instabilities or shapes that do not meet storage or safety requirements of SPR caverns. Some evidence of incomplete mixing has been observed in laboratory studies of mixing and leaching. However, experience from the field operations is that uniform dissolution occurs in caverns suggesting mixing is complete. This observation is supported by validation of the Sandia solution-mining software (SANSMIC) against field measurements of cavern shapes—SANSMIC assumes complete mixing. The apparent discrepancy about the degree of mixing between raw water and brine is thus a focus of this report.

This report has four major sections:

1) problem statement and scope (Section 2);
2) background and literature review on SPR leaching operations, models of leaching, field measurements of leaching and cavern shapes, and laboratory experiments of mixing and/or leaching performed at SNL (Section 3);
3) recent laboratory experiments in 2014–2016 on flow visualization of processes governing poor-to-well mixed conditions (Section 4); and
4) discussion, implications, and suggestions for field activities and future laboratory and field investigations to address research gaps (Section 5).

We find that completely-mixed conditions most likely occur in regular field operations at SPR in tall and cylindrical caverns, based on review of cavern measurements, SANSMIC modeling, and temperature and density wire-line logging. Some laboratory studies from previous SNL studies exhibited a flaring-upward geometry of dissolved salt walls, but it is uncertain if this indicates incomplete mixing and localized leaching. The recent laboratory experiments in 2014–2016 found that the collision of the injection jet against the bottom of a tank, which represents a SPR cavern, lead to greater mixing. We therefore suggest collision of a jet against the bottom of an SPR cavern may improve mixing in wide caverns, which can be a focus of future studies. Only incomplete mixing and ponding of fresh water was observed only at low flowrates and short travel distance from the injection depth to the upper air-brine interface (which represented the oil-brine interface). Travel of incompletely-mixed water up an injection string still tends towards mixing as the boundary layer flow separates and mixes after the distance of several injection diameters away from the injection depth. Thus, SPR operations outside the normal range may contribute to incomplete mixing, such as low injection rates and short distances between the injection depth and the OBI. Although these conditions are infrequent in SPR's operational history, they may become be important in future operations related to cavern management.

2. PROBLEM STATEMENT AND SCOPE

Mixing of injected raw (fresh or undersaturated) water and brine affects dissolution of the walls in salt caverns of the U.S. Department of Energy's Strategic Petroleum Reserve (SPR). Complete mixing throughout the cavern leads to even dissolution of caverns walls above the injection depth. Even dissolution is desirable for solution mining of mechanically stable cavern shapes, especially cylinders. Poorly-mixed fresh water could potentially cause undesirable and non-uniform dissolution (hereafter termed "leaching"). Ledges could potentially be leached if buoyant fresh water collects and locally leaches under the oil-brine interface (OBI; Figure 1; Khalil and Webb, 2006). Localized cavern widening could lead to salt fall. Non-uniform leaching could adversely affect cavern mechanical stability for caverns near the edge of a salt dome or caverns undergoing multiple oil-withdrawal cycles. Non-uniform leaching and resultant irregular cavern geometries may also affect available volumes for oil storage. Injection of raw water occurs during the following: initial solution-mining of caverns in the geologic salt domes; remedial leaching operations to increase cavern volume or alter and maintain cavern shape; or oil drawdown. Oil drawdown involves injection of raw water into saturated brine at the bottom of a cavern in order to drive oil upward and out through a production pipe. Thus, knowledge on conditions that control incomplete-to-complete mixing of raw water and brine is important for quantitative planning of the various leaching scenarios. However, operating conditions and cavern properties under which incomplete mixing may potentially occur are not well understood.

The purpose of this report is to present current understanding on the controls of incomplete-to-complete mixing between raw water and brine in SPR salt caverns with implications for leaching. Previous laboratory studies at Sandia National Laboratories (SNL) focused on generating data for validation of solution-mining software. These studies did not explicitly focus on understanding conditions that govern poor to well-mixed cavern conditions. These studies were typically scaled for various standard leaching operating conditions of SPR caverns and had a narrow range of examined conditions (e.g., flowrates and injection depths). This report reviews and investigates the set of factors that may cause incomplete-to-complete mixing and what knowledge gaps remain. We synthesize direct and indirect information on mixing from previous field, modeling, and laboratory studies. We present new laboratory experiments that investigated the influence of previously uncharacterized factors, including how the contact of injected water (the water jet) with the base of a cavern may enhance water-brine mixing. We discuss additional novel experiments that examined upward flow of poorly-mixed buoyant water near the injection pipe to determine if this could lead to pooling of fresh water under the OBI. Our findings support the occurrence of complete mixing during typical SPR operating conditions. Non-standard operating conditions, especially low flowrates and short travel distances from the raw water injection depth to the OBI, would have to exist to cause poor mixing and associated preferential leaching.

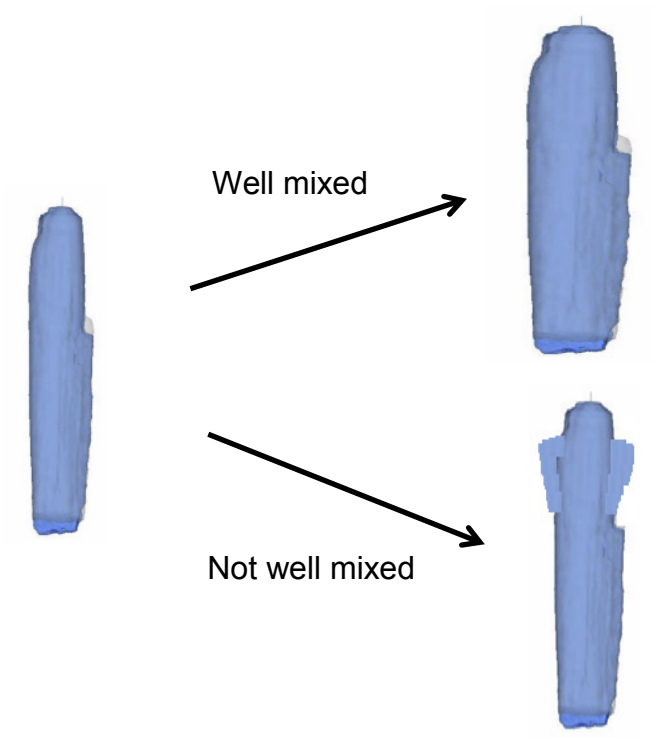

Figure 1. Schematic of hypothesized potential cavern shapes under well-mixed or poorly-mixed conditions between injected raw water and brine in SPR salt caverns.

3. BACKGROUND AND PREVIOUS WORK

Mixing of injected raw and brine in salt caverns is part of a sequence of events and processes that occur during leaching operations or oil drawdown at SPR. This sequence is stated here to provide the reader context on the mixing itself and its place in SPR field operations. The sequence is:

1) injection of raw water, with possible brine production depending on leaching operations or oil drawdown scenarios;
2) mixing of raw water and brine in the salt cavern, followed by transport of the mixture or potentially poorly-mixed raw water within the cavern to the salt cavern walls and upward to the oil-brine interface if there is an upper oil cap or stored oil;
3) contact of the mixture of water and brine or poorly-mixed water at the salt cavern wall and dissolution of the salt; and
4) change in cavern size and shape due to salt wall dissolution—the outcome of leaching.

Injection of raw water occurs under a variety of leaching operations or oil drawdown scenarios, each of which may affect the mixing process. Injection flowrate, injection depths, and pipe diameter are operational parameters that affect mixing. Thus, we begin our discussion with a summary of cavern leaching operations, including definition of common field-operation terms (Section 3.1). We highlight how the operations may affect mixing, dissolution of salt cavern walls, and the change in cavern size and shape. To assess the current understanding of mixing processes based on previous work, we next discuss mathematical leaching models and field observations (Section 3.2)—highlighting direct or indirect evidence for the type of mixing (i.e., incomplete to complete mixing). As discussed below, field observations of cavern shape by sonar and wireline logging of density and temperature suggest well-mixed conditions for remedial and oil drawdown cases. Field observations do not directly observe the mixing and leaching processes, and thus SNL has conducted many laboratory experiments to generate data for validation of solution-mining software. We discuss what was learned from the laboratory experiments to set the stage for presentation of recent laboratory studies conducted by the authors in 2014–2016. The new work directly examines what controls the transition from poor-to-well-mixed conditions with a focus on spreading of a water jet against the bottom of a tank (simulated cavern; Section 4.1) and the flow of poorly-mixed water up the injection pipe (Section 4.2).

3.1. Cavern Leaching Operations

Salt solution mining is the mining of salts by dissolution using undersaturated water (Warren, 2016). It is used by the SPR to develop and maintain underground storage caverns in salt domes that store crude oil. Leaching refers to the dissolution process itself and extraction of the solid salts—a key part of solution mining operations. The capability to simulate and accurately predict leaching is vital for managing the caverns through decades of service. Leaching depends on the saturation level of water that contacts the salt cavern walls; thus, mixing between injected raw water and brine in the caverns plays a major role in dissolution. During leaching, water that is undersaturated in salt comes in contact with and dissolves the salt exposed at the cavern walls, thereby increasing and modifying cavern volume and geometry. The degree of leaching affects both the cavern size and volume available for oil storage. Leaching also affects salt cavern

geometry. Non-uniform dissolution has the potential to create non-cylindrical caverns shapes (Figure 1), which could mechanically destabilize the cavern. Hence, understanding the role of mixing on dissolution on effects on cavern volume and shape is import to accurately design or maintain caverns during SPR leaching operations or oil drawdown.

The following three types of solution mining are used at SPR: bottom-inject (direct); top-inject (reverse); and oil drawdown (Weber et al., 2014; Weber and Rudeen, 2015). Bottom and top injections each involve two pipes (also called "strings")—either as separate wells or in a concentric configuration in a single well—through which raw water is injected and brine is extracted (produced; Figure 2). During bottom-inject solution mining, raw water is injected below the depth that brine is extracted. Injection and extraction both occur below the depth of the buoyant oil, if oil is present in the cavern. Oil can be involved in creation of caverns and during remedial solution mining to control where undersaturated water contacts the salt walls and is referred to as "blanket oil"—the blanket oil floats on top of the brine and prevents mixed water and brine from contacting the salt walls. In bottom or top-inject configurations, extensive dissolution and recession of the salt walls occurs at the depth where the undersaturated aqueous fluid mixture contacts the salt walls for the longest duration throughout the entire leaching process. Typically, the pattern of salt-wall leaching tapers to the production string depth and then is relatively uniform in diameter between the production string and the oil-brine interface (OBI). The uniform dissolution is thought to be due to completely-mixed conditions between the water and brine. The amount of leaching and salt wall recession depends on the distance between the injection and extraction depths and the relative position of the OBI. The OBI may be stationary or moving if there is concurrent oil injection (Weber and Rudeen, 2015). Bottom-inject leaching is used for the early phases (sump and chimney) of new cavern development.

The top-inject case also involves two hanging strings located below the OBI, but in contrast to the bottom inject case, the raw water is injected above the level that brine is extracted. Similarly to the bottom-inject case, extensive leaching occurs near the injection depth and then tapers between the injection and extraction levels. The amount of leaching in a given region of the salt wall also depends on the distance between the injection depth and the OBI, as well as the relative location of the brine extraction. Oil can be simultaneously injected for this configuration in a process called "leach-fill." Top-inject solution mining is used at SPR for cavern roof development and volume expansion. In either bottom- or top-inject cases, completely-mixed conditions are assumed between the injected raw water and brine. Poorly-mixed conditions, for example, would be a case where fresh water ponds under the OBI or the raw water and brine are otherwise stratified in the cavern. The conceptual model of stratification, as discussed below, does not seem to occur in the field under standard leaching operations.

In the oil drawdown case, a single string is used to inject water below the OBI in a cavern that is mostly full of oil. For a full cavern, the oil is approximately 10 to 40 ft from the bottom of the cavern. The oil is displaced upward and out of the cavern through the slick well. The OBI moves upward toward the cavern roof during oil drawdown and leaching occurs below that level. The typical leaching pattern consists of extensive leaching near the injection depth, tapering to near zero at the final OBI depth (Weber et al., 2014). For the high flowrates (100,000 bbl/day or Reynolds number (Re) of ~ 10^6), completely-mixed conditions are assumed near the injection depth.

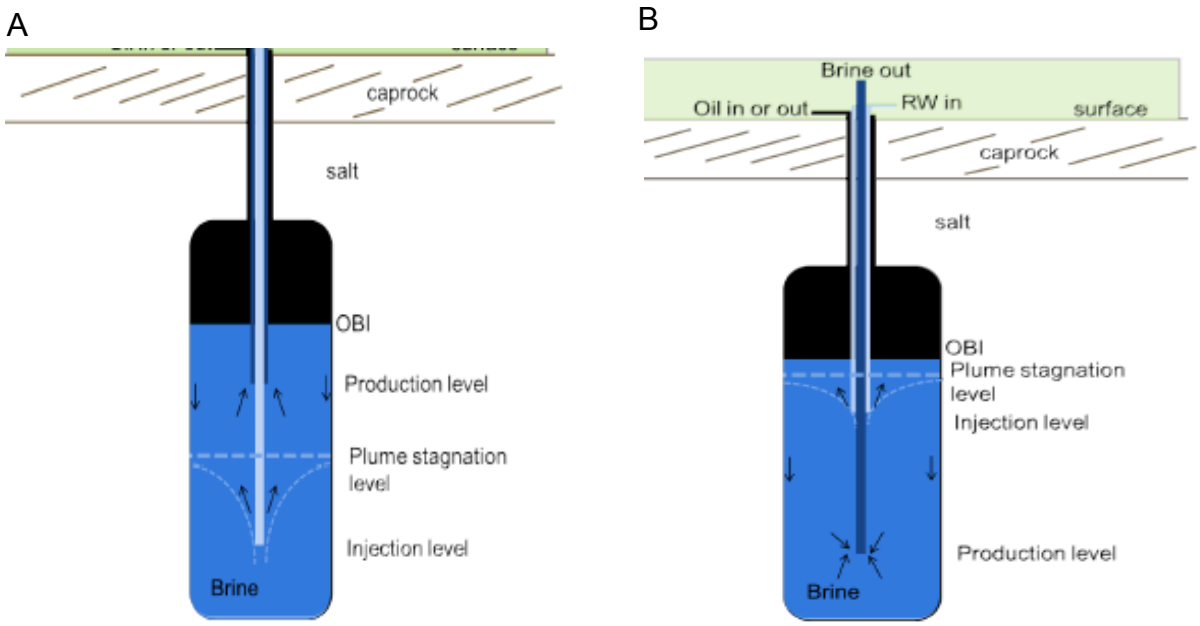

Figure 2. Leach configurations for A) bottom-inject (direct) and B) top-inject (reverse) leaching (after Weber, 2015).

Remedial leaches are performed at SPR to maintain existing caverns rather than develop new ones. Remedial leaches occur below a volume of stored oil and can involve bottom- or top-inject leaching. Remedial leaches are used to counter creep closure and maintain or increase cavern volumes for storing oil (Weber et al., 2013). Remedial leaches also can be used to alter cavern shapes (e.g., leaching to improve cylindrical cavern shape). Completely-mixed conditions between raw water and brine are desired when designing and performing remedial leaching. Non-standard operations, such as inadvertent string breakages, well clogging or other causes of low injection flowrates, or wide caverns and short travel distances to the OBI may promote poor mixing and possibly non-uniform leaching. The impact of non-standard operations on mixing and leaching is not well understood or quantified from previously studies at SNL.

The impacts of low flowrates on mixing and the type of leaching (e.g., uniform versus non-uniform) are not well understood, as the three types of leaching are typically performed at high flowrates (on the order of 100,000 bbl/day or *Re* of approximately ~10^6); however, a recent remedial leach was performed at a relatively lower flowrate (25,000 bbl/day or *Re* of ~ 230,000; L. Eldredge, pers. commun., Feb. 1, 2016). The flowrates and *Re's* will cause these jets be to fully turbulent (using the rule of thumb of jets being fully turbulent at *Re* > 10^4; Dimotakis, 2000; Webb, in review). SPR does not have any SNL reports that document low flowrate jets in the non-turbulent or transition regime. For all leaching types, the typical leach pattern occurs when the wall is uniformly dissolved from exposure to completely-mixed, undersaturated brine. By "completely-mixed", we mean that the concentration of salt in the aqueous fluid essentially

has no spatial gradients—the aqueous fluid is constant, or close to being constant, in dissolved salt concentration.

Uniform leaching and design of the leaching programs, include that of oil drawdown over many fill and drawdown cycles, is expected to generate and maintain cylindrical caverns, a shape that is structurally and mechanically stable in a salt dome (except for creep closure). However, there are factors that can influence the leaching process and patterns of salt wall recession from the ideal radially symmetric, cylindrical cavern geometry. Such factors include: local variances in salt structure, salt composition, and solubility; operations and issues including string breaks and well clogging; and potentially effects on raw water and brine mixing and leaching by pre-existing cavern geometry (e.g., wide caverns versus long, slender caverns). One potential source of non-uniform leaching is salt wall exposure to poorly-mixed raw water. If the raw water is poorly mixed, local salinity gradients may exist at the cavern wall that may leach the areas in contact with a lower-salinity aqueous fluid to a greater extent than other areas of the salt wall in the cavern. Ponding of fresh water under the OBI would be an example of stratification of fresh water and brine that could lead to localized leaching. For the oil drawdown case, over the repeated oil fill and drawdown cycles that occur during the lifecycle of the cavern, non-uniform leaching would result in an irregular cavern shape that deviates significantly from the symmetry of a cylinder and is therefore mechanically unstable. It is hypothesized that such irregular shapes may include "undercuts" immediately below the OBI, which would be a narrow horizontal zone of concentrated leaching that deviates from the rest of the cylindrical shape of the cavern. Another possible geometry is an upward flaring, similar to a morning-glory flower—this is seen in laboratory studies (see Section 3.3)—again, a deviation from the ideal cylindrical geometry.

As leaching is a consequence of the salt saturation level due to raw water and brine mixing, models of leaching make assumptions about mixing. These are discussed next to show how well certain mixing assumptions are able to reproduce observed cavern shapes. Thus, the modeling is indirectly providing insight into the mixing and leaching processes through validation to field cavern shapes. SPR uses leaching models to determine how solution mining operations and conditions control leached cavern governs. Factors involved include: the injected raw water specific gravity and temperature; injection rate, duration and depth of injection; brine extraction rate and depth; depth of the oil-brine interface; and salt properties (e.g., salt composition and insoluble material quantity and distribution). Prediction of cavern geometry is important to: produce mechanically stable caverns, maintain the "webbing" distance between caverns, and keep the desired distance between a cavern's walls and the edge of the salt dome. These relationships are complex and not explicitly known, and thus, knowledge gained from a combination of operational experience, laboratory experiments, and simulation is necessary to develop, maintain, and operate SPR caverns (Weber et al., 2014).

3.2. Cavern Leaching Models and Measurements

SPR uses the Sandia Solution-Mining Code (SANSMIC) to understand what can be controlled (e.g., flowrate, injection depths, etc.) to obtain a desired cavern shape. This software makes assumptions on raw water and brine mixing that strongly affect the predicted cavern shape. Knowledge of these assumptions and their limitations is important for SPR to plan the variety of leaching operations and to know if the software needs updating. SANSMIC can simulate standard bottom- and top-inject leaching and oil drawdown discussed in Section 3.1, which includes cavern leaching, salt-wall recession, and mixing of injected raw water and brine (Weber et al., 2014). SANSMIC informs SPR cavern leaching design and operational decisions in order to ensure that caverns achieve or maintain desired shapes, volumes, and mechanical stability, and system hydraulics.

SANSMIC addresses the main processes of leaching operations, including: 1) raw water injection and mixing with ambient brine; 2) transport of the aqueous mixture to the cavern wall; and 3) salt wall recession by dissolution of the undersaturated aqueous fluid at the salt cavern wall (Weber and Rudeen, 2015). SANSMIC treats these processes sequentially (Russo, 1981; Weber et al., 2014). The conceptual model of leaching underlying SANSMIC begins with raw-water leaving the injected string as a turbulent jet that travels toward the cavern floor. After the jet reaches a maximum depth of penetration, the low-salinity water, being lighter than the saturated-ambient brine, starts to rise toward the cavern roof as a turbulent plume. All the while, turbulence acts to mix the low- and high-salinity fluids, creating an intermediate salinity mixture in the plume that spreads toward the cavern walls as it rises. Once the undersaturated plume reaches the cavern wall, dissolution of the wall begins with salt wall recession. As more raw water is injected, mixed, and transported to the wall, the vertical extent of the dissolving region grows. The vertical depth of dissolution and salt wall recession is the maximum plume height to the location that the plume contacts the salt wall.

SANSMIC uses three basic components to quantify that conceptual model: 1) a jet-plume model; 2) an advective-diffusive mass balance equation to describe the aqueous mixture and dissolved transport to and from the wall; and 3) a model of the rate of salt wall recession (Russo, 1981, 1983; Weber, 2015). The jet and rising buoyant plume are treated as unconfined and steady. In both the jet and plume, turbulent mixing is assumed to be rapid enough to prevent cross-sectional gradients in salinity (specific gravity) and velocity. Thus, concentration in the plume is assumed to be spatially uniform. SANSMIC uses the jet model to calculate the maximum jet penetration depth, and the plume model to calculate the maximum penetration height of the plume. Key assumptions related to leaching processes include the spatially uniform salt concentration in the jet and plume and axisymmetric shapes of the caverns, jet, and buoyant plume.

SANSMIC has been validated for a number of scenarios including cavern-scale cavern development (Eyermann, 1984), bench-top-scale leaching and withdrawal (Reda and Russo, 1983; Russo, 1983; Reda and Russo, 1984; Lord et al., 2011; Weber et al., 2014), and most recently, cavern-scale oil withdrawal (Weber et al., 2014). By capturing the change in cavern volume over time and final cavern shape, SANSMIC is likely capturing the physics of raw-water mixing and subsequent salt wall dissolution involved in these scenarios. As a point of reference for discussing SANSMIC assumptions, we focus on oil drawdown. SANSMIC has been used to

simulate data from the 2011 sale of oil from the SPR. This sale provided the highest quality data to date on injection and production rates and cavern shapes for the oil drawdown scenario. As presented by Weber et al. (2014), SANSMIC predications of cavern radius with height were within 2% of the values measured in specific SPR caverns using sonar (Weber et al., 2014). Ideal leaching patterns (via uniform leaching)—extensive leaching near the injection string depth that tapers up to the final OBI depth—were predicted by SANSMIC and observed in the sonar record. The total volume leached during withdrawal was estimated by SANSMIC within 8% of the value estimated from the sonar record.

In addition to oil drawdown, Weber et al. (2014) also used SANSMIC to simulate cavern-scale top- and bottom-inject scenarios and compared the results with field measurements. From our assessment of the SANSIC revalidation study by Weber et al. (2014), we do not observe cavern shapes such as "undercuts" or "morning-glory" geometries that would be attributable to poorly-mixed plume dynamics. SANSMIC seems to accurately (with the uncertainty mentioned above) capture the cavern shapes, suggesting that the fully-mixed plume assumption is valid. At first glance, some shapes may suggest "undercuts" due to poor mixing, but explanatory causes for these shapes are given such as salt-fall (e.g., see page 28, Weber et al., 2014). String breaks or cuts may have focused leaching over a short vertical distance, but SANSMIC prediction of cavern radius for these cases is still reasonable.

In summary, SANSMIC seems to capture well the cavern shapes from withdrawal, direct-inject, and top-inject scenarios based on historical and recent field data. Note, however, that these validation cases focused on tall, slender caverns, typically under high flowrate conditions (fully turbulent jets; average flowrates of ~ 25,000 to ~140,000 bbl/day for the variety of bottom-inject, top-inject, and oil drawdown scenarios; Weber et al., 2014). Non-uniform leaching may still be a question for remedial or drawdown leaching in wide, short caverns or under lower flowrates and short distances from the injection string to the OBI. SANSMIC also does not address affects on mixing due to impact of the injection jet against the bottom of the cavern, hereafter referred to as impingement. Such impingement may affect spreading and mixing of the plume, as discussed in Section 4.1.

3.3. Raw Water and Brine Mixing Laboratory Experiments

Sandia National Laboratories has conducted laboratory experiments since the early 1980s to generate data for validating solution mining solution and to understand raw water-brine mixing and/or leaching processes that may occur in full-scale SPR caverns. Water-brine mixing and leaching are processes that can be directly studied in the laboratory, but are difficult to directly observe in the field. Laboratory experiments were conducted to elucidate the relationships between water injection, water-brine mixing, transport of the mixed aqueous fluid to the wall, and the associated salt dissolution and resultant salt wall shapes.

To overview this subsection and its context in the rest of this report, we first define similitude concepts and dimensionless numbers used for physical models of water-brine mixing and salt dissolution that are used to scale the field processes down to the laboratory scale. The dimensionless numbers are also useful to compare laboratory studies in terms of processes that govern the flow and mixing processes. Flow and mixing processes also occur within the oil, but

are beyond the scope of this report. Qualitative laboratory behavior may still be useful for understanding the physics of field scale mixing and leaching even if the scaling relations are not perfectly matched, as discussed below. We primarily focus on work performed at or for SNL. We compare general laboratory findings to cavern leaching simulations and field observations, including cavern shapes. We then discuss the motivation for the most recent experiments performed in 2014-2016, which are discussed in Section 4.

Similitude is a concept that ensures laboratory-scale processes operate sufficiently similarly to field-scale cavern processes such that cavern observations can be understood or inferred from laboratory-scale results. Depending on the processes or behavior of interest, it is necessary to consider one or more of the three types of similitude: geometric, kinematic, and dynamic. Geometric similitude consists of having the same angles and length-scales controlling processes at the laboratory and cavern scales. Geometries of interest for SPR caverns include the depths of injection and production, the diameters of production pipes or tubes, and the cavern heights and diameters. Similarity is expressed as a dimensionless ratio of length scales. For geometric similarity the dimensionless number is expressed as:

$$L = \frac{L_{cavern}}{L_{lab}} \tag{1}$$

where L_{cavern} is a length at the cavern scale and L_{lab} is a length of the laboratory-scale system. Typical SPR caverns are cylindrical and slender at approximately 700 m (2297 ft) high by 70 m (229.7 ft) diameter (Voropayev et al., 2012)—the height to diameter ratio is 10. Typical injection pipe diameter is 0.25 m (9.85 inch).

Kinematic similitude relates the scales of motion and involves the variables of time, velocity, volumetric flow rate, and acceleration. Kinematic similitude is neglected in this problem as dynamic similitude is thought to be more important. Dynamic similarity relates the dominant forces driving the fluid motion. For SPR caverns, the mixing of a raw-water jet and brine involves both momentum and buoyancy forces. Similitude in this case is described with the densimetric Froude number, *Fr*, which is defined as the ratio of momentum to buoyancy forces and expressed as follows:

$$Fr = \frac{\rho_{raw} U^2}{(\rho_{raw} - \rho_{brine}) g d} \tag{2}$$

where ρ_{raw} is the density of the raw injected water (fresh or undersaturated); ρ_{brine} is the density of the ambient brine in the cavern (or other container of the laboratory model); U is the velocity of the injected raw water jet; g is gravitational acceleration; and d is the injection pipe diameter. On average, *Fr* equals 27 for jets in SPR caverns, based on a typical operational volumetric flowrate of 0.18 m^3/s (100,000 bbl/day), jet velocity of 12.5 m/s, 0.25-m (9.85-inch) diameter pipe, raw water density of 992.2 kg/m^3, and saturated brine density of 1191.4 kg/m^3 (at 40°C).

Another important similarity variable for the raw-water jets is the Reynolds number, *Re*, which is defined as the ratio of inertia to viscous forces, and expressed here as follows:

$$Re = \frac{\rho_{raw} U d}{\mu_{raw}} = \frac{U d}{\nu_{raw}} \tag{3}$$

where μ_{raw} is the raw water dynamic viscosity and ν_{raw} is the kinematic viscosity ($\nu = \mu/\rho$). On average, $Re = 1.4 \times 10^6$ for jets in SPR caverns, based on the same values of volumetric flowrate, jet velocity, and injection pipe diameter as the average Fr estimate above and μ_{raw} of 6.53×10^{-4} kg/m-s (at 40°C). As long as the flows in both the laboratory and field studies are fully turbulent and the jets have Re on the order of 10^4 or greater, the gross flow physics should be similar and independent of the value of Re. Ideally, Re_{cavern}/Re_{lab} and Fr_{cavern}/Fr_{lab} would both equal one, indicating the laboratory experiments were matched or analogous to the cavern scale. However, matching both Fr and Re is difficult in the laboratory and would require use of injected fluids of different viscosities or a length ratio of one. Instead, SNL laboratory experiments typically match Fr.

The first set of SNL-conducted laboratory experiments on leaching focused on leaching associated with oil drawdown (Reda and Russo, 1983; see Table 1 for a summary of the experiments). Major goals were: to determine if oil would adhere to and/or penetrate into salt cores and thereby prevent undersaturated water from contacting the salt walls of the cavern; measure the transient salt wall recession due to salt wall leaching, in pressurized salt cores (at 13.8 MPa); and measure leached salt wall shapes to support validation by numerical modeling. Gamma-beam densitometry was used to measure salt wall recession rate and the possible presence of an oil film after passage of the OBI. Cavities were cored into the salt cores where the raw water-brine injection was performed, thus the cavity is meant to represent the field cavern. Cavity radius was also measured sectioning-micrometer techniques after leaching as a check on the gamma-beam methods. The cores were 22.86 cm (9.00 inch) tall by 9.17 cm (3.61 inch) outer diameter, with a machined hollowed cavity 20.32 cm deep (8 inch). Top- and bottom-inject leaching was investigated, with the raw water injection and brine production at the top and bottom of the salt cores. Bottom-inject and top-inject scenarios without oil were also investigated (Reda and Russo, 1984).

The salt-leaching tests showed salt walls flaring upward or "morning-glory" flower-like shapes (Figure 3) for $Re = 400$ and $Fr = 195$ without oil, and $Fr = 86–975$ and $Re = 6–771$ with oil, with the greatest flaring for the top-inject case (Figure 3B). The oil-drawdown cases exhibited "undercuts" in the cavity wall at the initial OBI, and possibly at the final OBI after drawdown ended (Figure 4; see red ellipse). The initial undercut was attributed to fresh water from the injection tube that was released into the cavity during initial pressurization up to 13.8 MPa (Reda and Russo, 1983). The gamma-beam measurements in the oil-withdrawal cases showed no evidence of an oil film and no salt-protection affect. These tests were at relatively low Re (86 to 975) compared to the field, with probably non-fully turbulent flows as would be expected for typical SPR operations. The key observations relevant to mixing are the flared geometry and the undercut. For the relatively low Re numbers, less mixing occurred in these laboratory experiments than would for field conditions, possibly leading to more of a flared-leached geometry than would be seen in the field for standard leaching and oil withdrawal scenarios. However, we have yet to establish a relationship between Re and mixing, which is further discussed in Section 4. These experiments also do not directly image mixing; thus, mixing processes can only be inferred. Evidence for non-uniform leaching was an initial undercut in the salt wall during the oil-drawdown case, not related to jet mixing. Again, as mentioned above, the undercut was assumed to have been created by exposure of the salt wall to fresh water that

Table 1. Laboratory experiments on mixing and salt dissolution.

Topic	Reference	Type of lab test	Process studied	Test conditions	Plume shape and mixing	Salt dissolution morphology
Water-brine mixing (around vertical tube and wide tank)	Saberian, 1973*	Bench scale: fresh water injection with dye into brine; wedge-shape containers 17 5/8" height by 23" radius; no oil used; salt wall used	Bottom-inject leaching	Inlet jet Re ≈ 3 Fr ≈ 7e-6	Approx. top-hat like with spreading under ABI**; counter flow away from salt wall	Dissolved wall morphology not discussed
Salt wall leaching and water-brine mixing	Reda and Russo, 1983	Bench scale: fresh water injection into cylindrical cavity in salt ~ 1-in radius by 8-in high; gamma-beam densitometer measurement of salt walls; no oil used	Oil drawdown, full-scale leaching, bottom-inject and top-inject leaching configurations	Inlet jet Re ≈ 400 Fr ≈ 195	Not measured; gamma-beam measured integrated fluid density and wall recession	Profile flares upward for bottom-inject and top-inject leaches (LH1; see their Figs. 4 and 5)
Salt wall leaching and water-brine mixing	Reda and Russo, 1984	Bench scale: fresh water injection into cylindrical cavity in salt ~ 1-in radius by 8-in high, with oil cap; gamma-beam densitometer measurement of salt walls; oil used	Oil drawdown withdrawal, moving oil-brine interface	Inlet jet Re ≈ 86 to 975 Fr ≈ 6 to 771.2	Not measured; gamma-beam measured integrated fluid density and wall recession	Flaring at initial lower OBI (due to fresh water to pressure up the experiment); minor flaring at top
Water-brine mixing	O'Hern et al., 2005, 2005a,b,c	Large tank: 35-inch diameter total, no salt lining, one test with oil layer	Oil drawdown, with two sizes of injection tubes	Scaled Fr to be equal to nominal cavern conditions	Planar laser induced fluorescence (PLIF) imaging	Some ponding under OBI/ABI, but low fresh water concentration
Salt wall leaching and water-brine mixing	O'Hern et al., 2010	Large tank: 35-inch diameter total, 25-inch ID lined with salt blocks; no oil used	Full-scale leaching, top-inject leaching, oil drawdown with ABI** rise and lowering	Scaled Fr to be equal to nominal cavern conditions	Temperature and conductivity profiles indicate regions of well mixing	Profile flares upward for top-inject leach; oil drawdown shows less flaring

*Non-SNL study

** "Air-brine interface"; no oil was used

leaked from the injection tube prior to the start of the jet flow. Such a process of leakage or low flow may not be relevant for field operations, but this is an example of a potential mechanism to generate non-uniform leaching. The transient spatially-distributed flow dynamics were not directly measured as the gamma-beam methods measured the attenuated beam through the salt and brine, thus giving a spatially-averaged measurement at a given depth. Thus, these studies suggest potential leaching patterns of the salt walls, but other techniques are needed to directly observe raw water-brine mixing.

To obtain additional data beyond the Reda and Russo studies (1983; 1984) for validation of numerical modeling of mixing and leaching processes, and to more directly observe mixing processes, SNL performed experiments of mixing and/or salt leaching in a large (35-inch) diameter tank and on smaller systems (O'Hern, 2005a, b, c; O'Hern et al.,, 2007; and O'Hern et al., 2010; Table 1). Also, as the undercut geometry of the oil withdrawal Reda and Russo (1984) may have been an artifact, additional information on leaching was desired (O'Hern et al., 2007). These SNL experiments used a variety of techniques to actively image the plume and salt wall recession. Small-scale tests include half-cylinder cavity in salt for imaging of bottom-inject salt leaching process (Figure 5). The flowrate was scaled to match a cavern flowrate 0.18 m^3/s (100,000 bbl/day). Results for a bottom-inject case showed an upper flared geometry (Figure 5C; see red ellipse). Testing in the large diameter tank involved cases with salt blocks lining the walls of the tank (Figure 6; O'Hern et al., 2010). Techniques to determine salt wall recession include ultrasonic transducers and pre- and post-test weighing of the salt blocks. Scaling was performed to match *Fr* between the tank and field scales. The scaled flowrate represented 100,000 bbl/day in the field. The post-test salt wall profiles (Figure 7) also show upward flared profiles.

In summary, the variety of laboratory experiments performed by SNL for SPR cavern mixing and leaching investigated a range of top-inject, bottom-inject, and oil-drawdown scenarios. These studies typically had relatively low *Re* and in some cases matched the *Fr* of the nominal SPR operational leaching case (100,000 bbl/day). The experiments typically exhibited flared profiles near the top of the salt cavern walls. The relationship between *Re*, *Fr*, flaring patterns, and raw water-brine mixing was not determined by these studies and warrants further study to understand laboratory-scale mixing and leaching and possible differences from field-scale observations (see Section 3.2). The field geometries of caverns discussed in Section 3.2 do not exhibit clear "morning-glory" or upper flaring or "undercuts" that can be attributed to poorly-mixed conditions (e.g., the undercut morphology is typically explained by salt falls in the field cases and not salt dissolution). These studies examined a small range of *Re*, were primarily focused on the jet and transport behavior rather than the return plume behavior, and were not able to address when to expect incompletely-mixed conditions in SPR caverns. To address that gap in our knowledge, experiments were performed at SNL to further examine conditions that produce incompletely or completely mixed conditions. The experiments examined the following situations: radial transport (spreading) of mixed fluid due to the jet impacting the bottom of the salt cavern and the lack-of spreading in upward flow near the injection string. These experiments are discussed in Section 4.

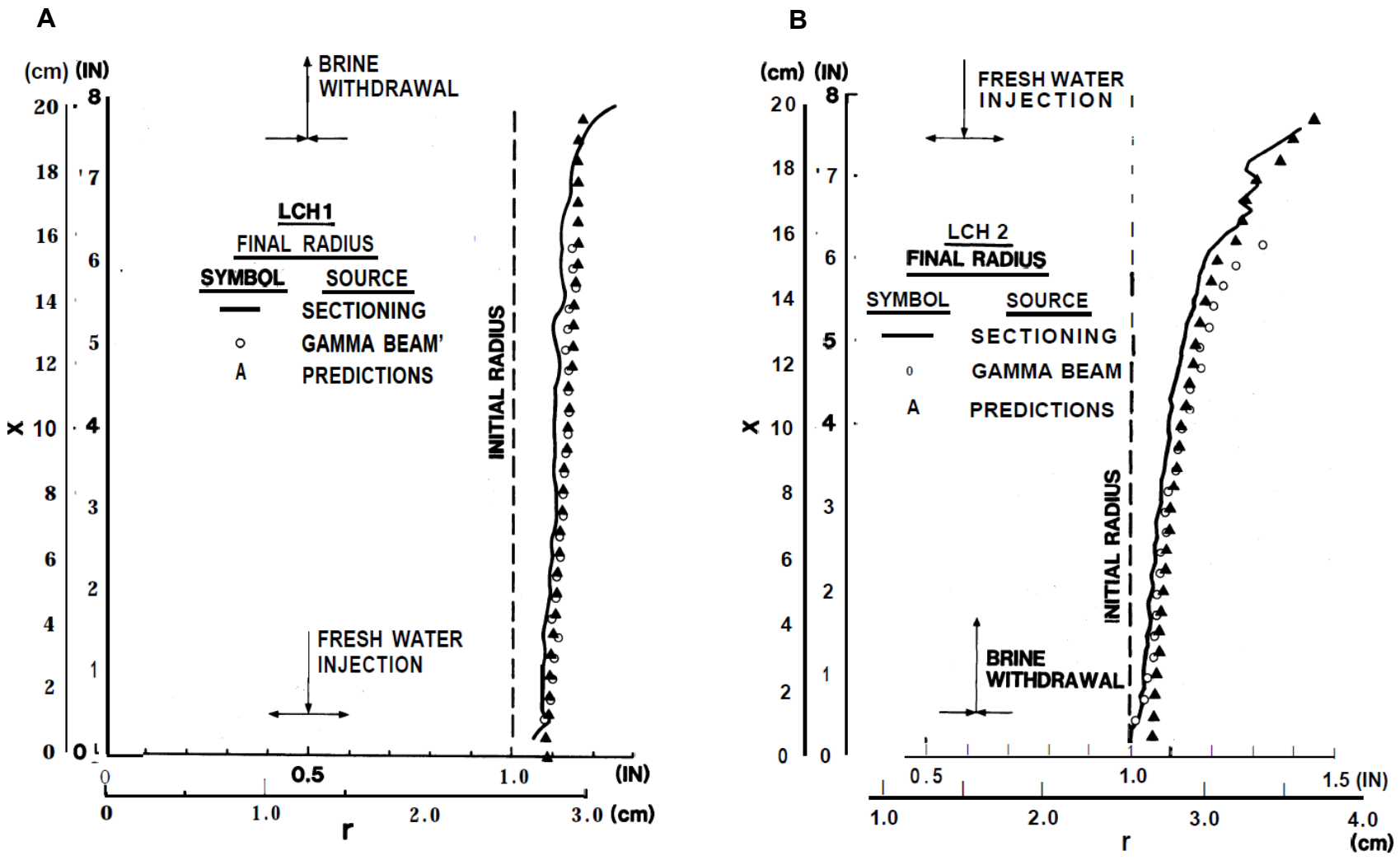

Figure 3. Salt cavity profiles by gamma-beam densitometry and sectioning-micrometer techniques for no-oil water-brine leaching experiments (after Reda and Russo, 1984). A) Test LCH1, a bottom-inject scenario. B) LCH2, a top-inject scenario.

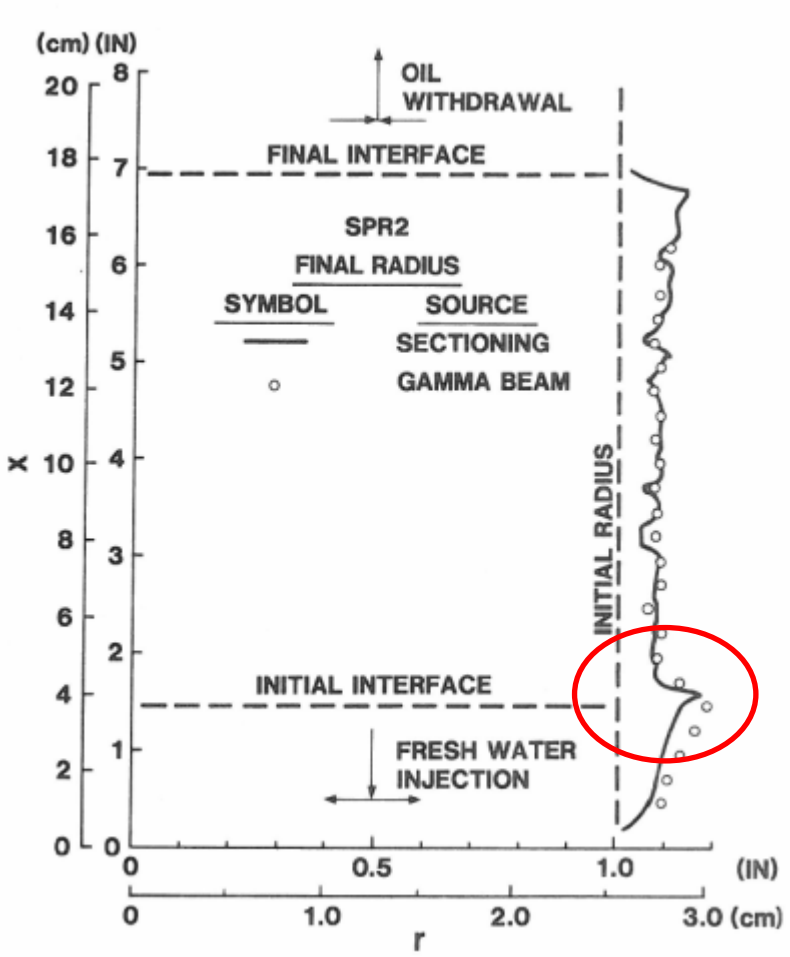

Figure 4. Salt cavity profile by gamma-beam densitometry and sectioning-micrometer techniques (after Reda and Russo, 1983). This is a representative oil drawdown example.

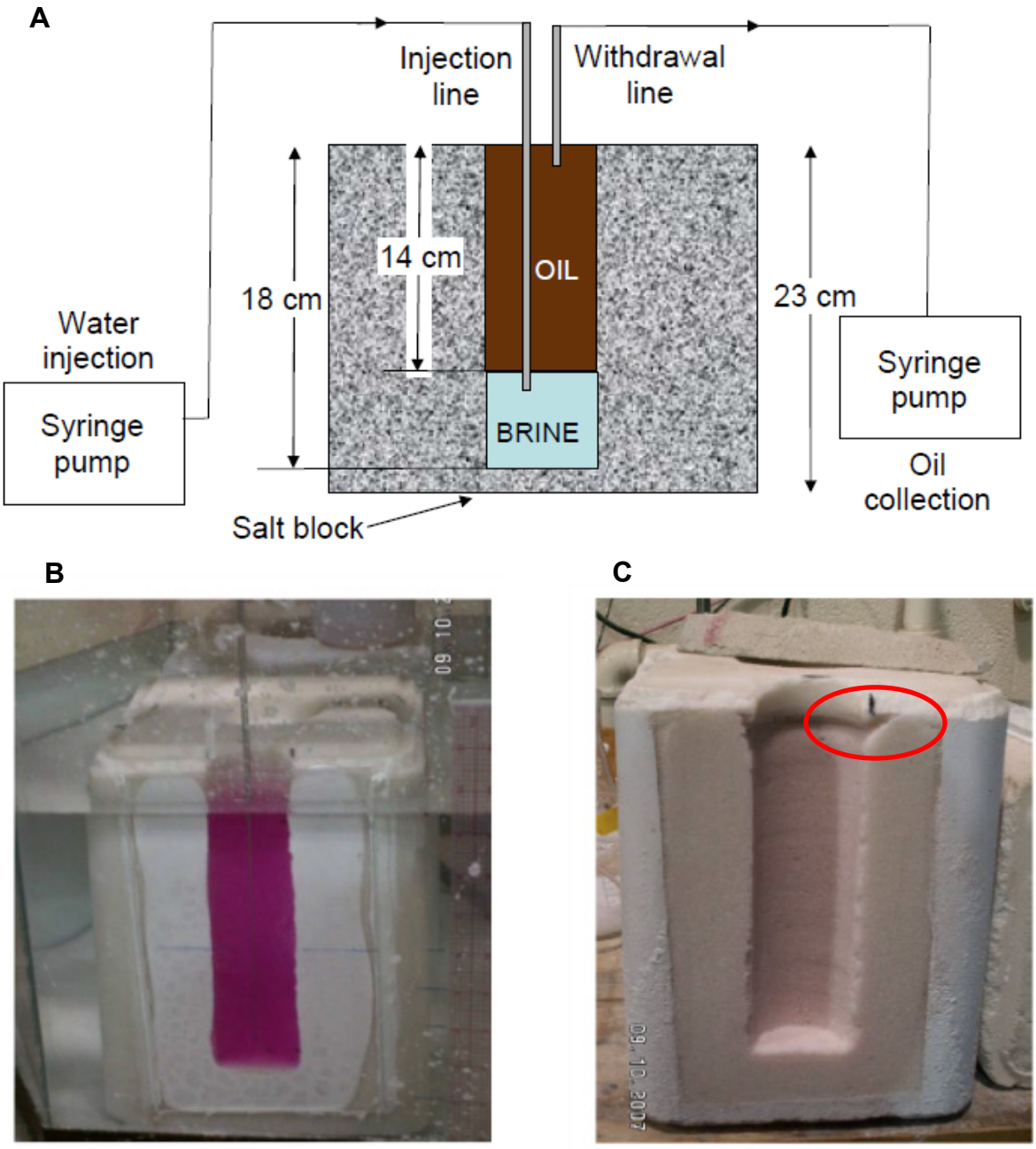

Figure 5. Schematic and images from leaching experiments in a half-cylinder geometry (after O'Hern et al., 2007). A) Schematic showing oil case. B) Image of a drawdown case. C) Post-test imaging of the salt leaching case showing upper-flared geometry.

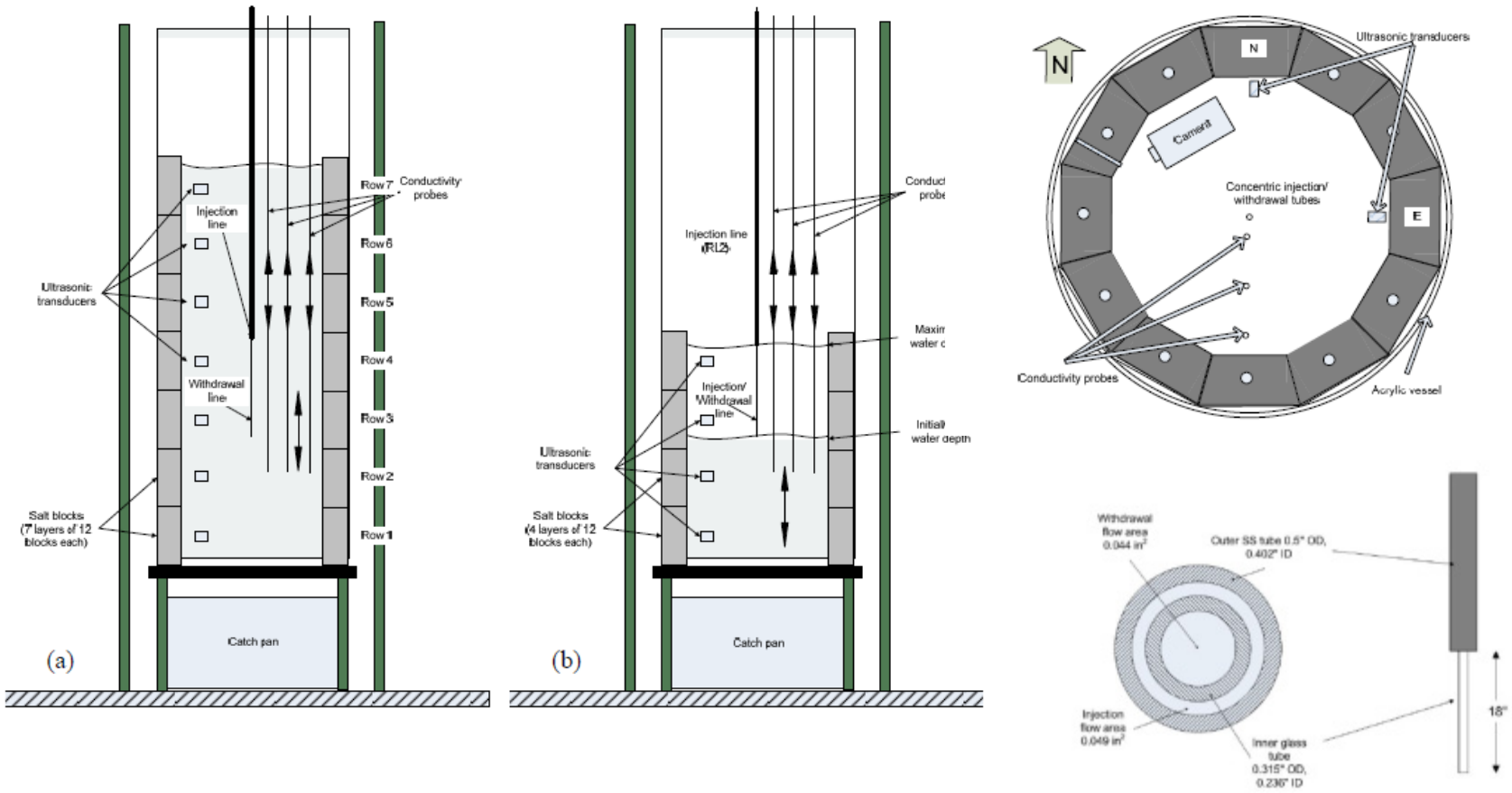

Figure 6. Schematics of the O'Hern et al. (2010) tank-scale experiments. A) Schematic of bottom-inject scenario. B) Schematic of oil-drawdown case. C) Concentric tubes used for injection and/or brine production.

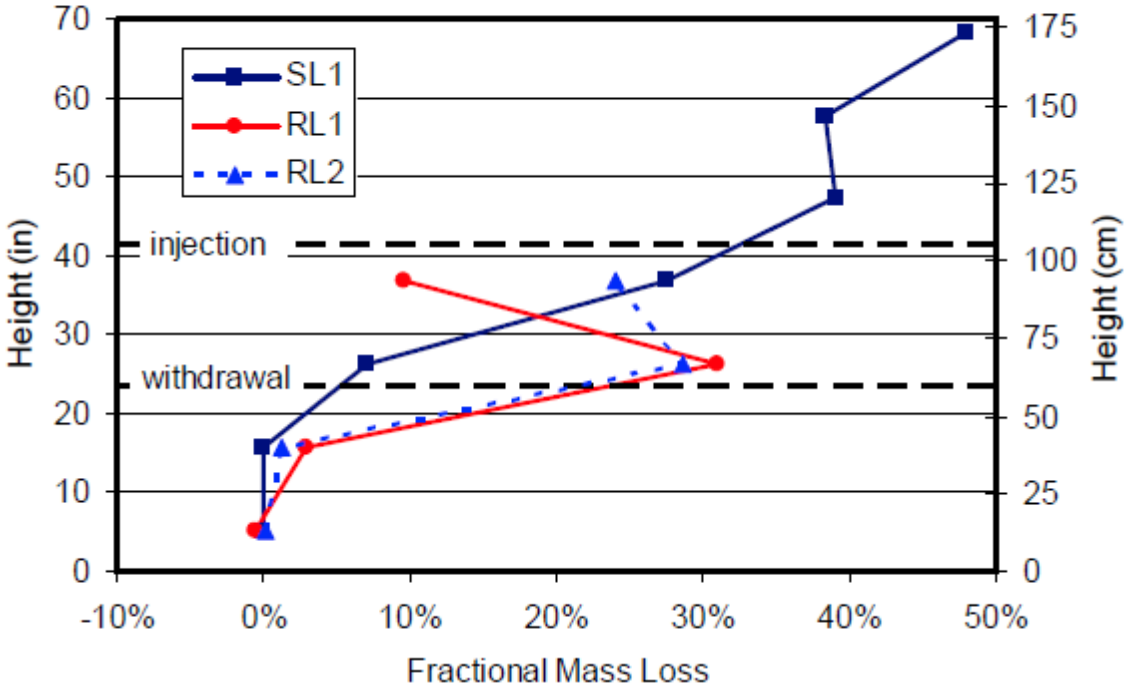

Figure 7. Mass loss as a function of height in the tank (from O'Hern et al., 2010).

4. RECENT LABORATORY EXPERIMENTS

Sandia National Laboratories performed additional laboratory experiments in 2014–2016 to examine raw water-brine mixing. These experiments had a more explicit focus on understanding incomplete-to-complete mixing between injected raw water and brine, as opposed to prior experiments that focused more on what mixing and/or leaching occurs when matching full-scale standard SPR conditions using similitude scaling relationships (see Section 3.3). The goal of the recent experiments was to gain insight into processes that may possibly lead to incomplete mixing in SPR caverns, including some non-standard flow conditions such as lower-than-typical flow rates of SPR leaching or drawdown operations.

A possible non-standard condition for leaching operations would be relatively lower flow rates (much less than the 100,000 bbl/day or *Re* on the order of 10^6—namely *Re* of 10^4 or less where transition or laminar flow may occur), which we hypothesize could contribute to poorer mixing. Knowledge on the occurrence of low flow rates has not been well documented. For example, data on the full range of flow rates and their durations for different operating conditions at the SPR has not been complied in previous SNL studies. Flow metering may also have a lower limit below which flow rates are not accurate and/or not measured. Flow rates as low as 1,000 bbl/day (Re ~ 10,000) could possibly occur while depressuring or repressuring the cavern (L. Eldredge, pers. commun., Feb. 1, 2015). A recent lower-than-standard flow rate remedial leach was done at approximately 25,000 bbl/day (or *Re* of ~ 230,000; L. Eldredge, pers. commun., Feb. 1, 2015). Drawdown and regular leaching is typically performed at higher flow rates on the order of 120,000 bb/day (Re of ~1.1×10^6; L. Eldredge, pers. commun., Feb. 1, 2015). Future activities at SPR may also involve remedial leaching in irregularly-shaped and/or wide, non-slender caverns, a situation for which the leaching models, like SANSMIC, are not yet validated. Aqueous mixing may occur differently in short and fat caverns, resulting in zones of poorly mixed raw-water and brine, motivating the need for a better understanding of mixing outside the normal range of operations in tall and skinny caverns. Knowledge on how to achieve complete mixing in wide caverns is needed—impingement of an injection jet with the bottom of a cavern may increase mixing as discussed in Section 4.1.

Section 4.1 focuses on imaging the raw-water jet over a range of laminar to turbulent flow rates for the purpose of understanding spreading of the jet and return plume (the "return plume" is defined below). A unique aspect, as compared to previous SNL experiments, is investigation and imaging of buoyant return plume spreading caused by the jet contacting and flowing along the bottom of the tank. Impingement of the jet with the bottom of caverns is possible, and its impact on spreading and well-mixed conditions should thus be investigated to further SPR's knowledge on controls on mixing. This work also broadens the range of flowrates considered in the previous laboratory experiments with relevance to leaching in SPR caverns. We found that for *Re* from 300 to 3000 and injection near the base of the tank, well mixed conditions occur—we did not observe ponding of poorly-mixed raw water at the ABI (equivalent to the OBI; we did not use oil in these experiments). Only when the raw water injection depth was close to the ABI, and at low flow rates, was raw water ponding at the ABI observed.

We therefore hypothesized that in the field, raw water banks at the OBI may form if upwardly traveling water via boundary layer flow occurs, especially for short travel distances and little

separation of the boundary layer flow. Section 4.2 therefore focuses on upward flow of initially poorly-mixed water in the vicinity of the injection tube. We found that the injection pipe may facilitate upward travel of poorly mixed buoyant water towards the OBI when flow rates are low and the distance is short between the injection location and the OBI—flow dynamics lead to growth of the boundary layer, separation of the boundary layer, and mixing.

4.1 Mixing of Impinging and Non-impinging Raw Water Jets in Brine

4.3.1. Introduction

The scenario of injection of low-salinity water into brine, restated in fluid dynamics terms, is that of the penetration of a negatively-buoyant jet into a miscible liquid. Here "negatively-buoyant" means that jet momentum and buoyancy act in opposite directions (Philippe et al., 2005). Downward injection of a lighter fluid into a denser fluid—or upward injection of a denser fluid into a lighter fluid—are examples of negatively buoyant jets. An example of a positively buoyant jet is thus injection of a denser fluid into a lighter fluid. Previous experimental work in the general literature has examined penetration and mixing behavior of high *Re* turbulent jets for negatively, positively, and neutrally buoyant conditions in wide or slender containers without impingement on a horizontal surface (Philippe et al., 2005; Voropayev et al., 2012; Nath et al., 2014); and the vertical impingement and spreading of turbulent negatively-buoyant jets on a horizontal surface with no effects of lateral confinement (Cooper and Hunt, 2007). "Impingement" is the collision of a jet with a barrier, which can divert the flow in a radial pattern (such as a radial-wall jet). Previous SNL studies (Section 3.3) have not investigated the collision of the injection jet against the bottom of SPR caverns—this is what we call bottom or basal impingement. However, such basal impingement may be a way to control the degree of raw water and brine mixing, which may be useful for wide caverns. For the oil drawdown case, the injection string is at least 10 ft above the base of the cavern, and typically up to 40 ft from it. Thus, for the high standard operation *Re*, jet impingement and spreading is likely and should be investigated to understand its effect on mixing processes.

The previous work on jets, in the broader literature, typically focuses on the geometry of the jet and plumes of the injected jet and entrained fluids, the evolution of the flow in time, and quantification of distances over which mixing occurs. Voropayev et al. (2012) observed and developed a theoretical model for the convection of the plumes (the mixture of the jet and brine) generated by negatively and positively-buoyant jets within a slender column. Their work did not consider basal impingement. Ahmad and Baddour (2015) studied vertical negatively buoyant jets and define the "minimum return point dilution" as the dilution occurring at the exit plane of the injection pipe. Ahmad and Baddour's work focused on the minimum return point dilution and did not quantify the return plume as it continued to travel along the injection pipe or tube. Flow beyond the minimum dilution point and continued mixing is of interest to SPR as mixing conditions at the OBI may govern preferential, non-uniform leakage, and thus receives focus in Section 4.2.

Section 4.1 describes new experiments on the mixing dynamics of both non-impinging and impinging negatively buoyant jets in a slender container, for a range of *Re*, by varying the depth of the injection and the injection flowrate. Of interest are conditions governing the degree of

water-brine mixing. These scaled laboratory experiments involve shadowgraph flow visualization using distilled water injected into brine with an upper free air-brine interface (ABI; no oil was used in these experiments). The metric for completely-mixed conditions in this study is when the width of the spreading plume of injected and entrained water equals the tank width. This work focuses on the mixing of the injected jet and brine near the base of the vessel, with fewer and more preliminary observations of the rising return plumes to the upper ABI. Results indicate stronger mixing of the water and brine with increased *Re* and impingement when the injection depth is located close to the tank base. However, for low *Re*, with injection still near the base of the tank, upward moving plumes are still well mixed by the time they reach the ABI. Only when the injection depth is placed near the ABI is a bank of poorly-mixed low-salinity water observed. To further understand the upward flow of poorly-mixed water, Section 4.2 examined upward flow along the injection tube, thus providing new data on return plumes beyond the point of minimum return dissolution (i.e., the location of the pipe outlet) of previous work.

4.3.2. Methods

Experiments were conducted within an acrylic rectangular tank with square cross section of 10.16 cm × 10.16 cm (4 in × 4 in) and height of 76.2 cm. An injection tube was placed through an opening in the top of the tank. The opening prevented pressurization of the upper head space. The brine column height was set to ~ 66 cm (26 in) at the beginning of each fluid injection period, giving an aspect ratio of 0.15. The ratio of injection nozzle diameter to tank diameter was 0.015, which is ~ 3 times that of a typical SPR cavern. Typical SPR caverns are cylindrical and approximately 700 m (2297 ft) high by 70 m (229.7 ft) diameter, with aspect ratio of 0.1 (Voropayez et al., 2012). Brine was removed from the top of the tank following subsequent tests to maintain the ~ 66 cm column height. New brine was used as necessary to maintain total dilution of the brine between tests to <10%. Figure 8 is a schematic of the tank, piping and injection tube, and the imaging setup.

The first set of results was performed with imaging near the base of the tank with a Phantom high speed camera under shadowgraph optics (Figure 8). Image resolution was 1200 × 1728 pixels, with up to 4058 frames per single experiment. Fifteen combinations of injection depths and flowrates were measured. A Harvard Apparatus PHD-Ultra series syringe pump supplied deionized distilled water into ~23 wt% NaCl solution at rates of 21.0, 52.5, 105.0, 157.5, and 210.0 ml/min (1.28, 3.20, 6.41, 9.61, 12.8 in^3/min), through a 1.55-mm (0.061-in) diameter 14 gauge EFD general purpose nozzle. These flowrates, the nozzle diameter, and the injected water properties resulted in jets with Re = ~300 to ~3000, whereas common production operations at SPR sites have jets with $Re = \sim 1 \times 10^6$ (see Section 3.2). Our intention is to investigate mixing behavior from relatively low-to-high Reynolds numbers (e.g., laminar to transitional or turbulent) to observe the range in possible incompletely-to-completely-mixed plume behavior. Imaging conducted near the base of the tank captured at least the tip of the nozzle at the greatest distance of the nozzle from the base of the tank (i.e., 7.62 cm or 3 in). Two opposing walls of the tank were oriented normal to the light path, and the tank was placed on a tilt table for horizontal leveling prior to all injection tests and imaging. Injection depths (distance of the nozzle from the base of the tank) were varied at 2.54, 5.08, and 7.62 cm (1, 2, and 3 in) for five flowrates.

For a second group of results, imaging was performed near the ABI, which was still maintained at ~ 66 cm (26 in). The injection depth location was maintained at 7.62 cm (3 in) from the base of the tank, with measurements at flowrates of 1.0, 5.0, and 21.0 ml/min (0.06, 0.31, and 1.28 in^3/min). A final measurement was performed with the injection depth located at 4.87 cm (1.92 in) from the ABI. Image processing and spatial measurements of jet and jet-brine mixture (i.e, width) were performed using Matlab.

4.3.3. Results and Discussion

Our results (Figures 9–14) capture important jet and brine mixing behavior near the base of the vessel, for impinging and non-impinging jets, including the relationship between *Re* and return plume width (e.g., Figure 14). We first summarize and discuss the major findings, we the details following in the rest of this section. Greater distances between injection depth and the bottom of the tank with higher flowrates cause greater mixing of the rising plumes for both impinging and non-impinging jet cases (see Figures 12–13), suggesting that low flowrates and low injection heights might lead to incompletely-mixed conditions. However, our results of imaging at the top of the tank indicate that even for low flowrates of 1 ml/min (Figure 15A), corresponding to the injection depth above the base plate of 7.62 cm (3.0 in), the rising plume appears completely mixed. For these injection depths near the bottom of the tank and the relatively low laboratory *Re* (<3000) compared to SPR standard field conditions of high *Re* ($\sim 1 \times 10^6$), the results still show complete mixing by the time the fluids reach the top of the tank at the ABI. We suggest that even low *Re* jets tend towards complete-mixing for long travel distances (greater than several diameters of the injection pipe or nozzle). Impingement causes greater spreading of the jet as it collides with the bottom of the tank and thus greater mixing of the return plume. For SPR applications, ensuring impingement with high flowrates and short distances to the bottom of the cavern may help to spread and mix the injected raw water—future work is needed for investigating if basal impingement will improve mixing in short, wide caverns.

In this study, only when the injection depth is approximately 4.87 cm (1.92 in) from the ABI does a bank of low-salinity fluid form (Figure 15D-F)—such a bank could possibly lead to "undercuts" or preferential leaching at the field scale in a salt cavern. Figure 15D shows the injection nozzle and assembly, which has sharp corners. It appears that boundary-layer fluid detachments occur at the sharp corners that initiate mixing; however, the travel distance is short to the ABI and thus the bank of low-salinity water still forms. We hypothesize that, in the field, fresh water banks may form if upwardly traveling water via boundary layer flow occurs. Boundary layer flow, or raw water that travels along the pipe with separation, and a short distance (e.g., due to string breakage) to the OBI thus may lead to ponding of fresh water (and lesser mixing), if this type of flow process actually occurs under field operations. Also, locations of positive curvature on the string may lead to flow detachment and greater mixing. Section 4.2 presents experiments on low jet *Re* for further examining flow of poorly-mixed raw water along the injection string.

Figure 9A–C display representative example image frames, of non-impinging and impinging jets, for two experiments out of the 15 combinations of injection depth and flowrate with imaging at the base of the tank (see Section 4.1.2 on Methods). Depending on injection depth and injection flowrate, plumes of water and entrained brine either never touch (or only touch for

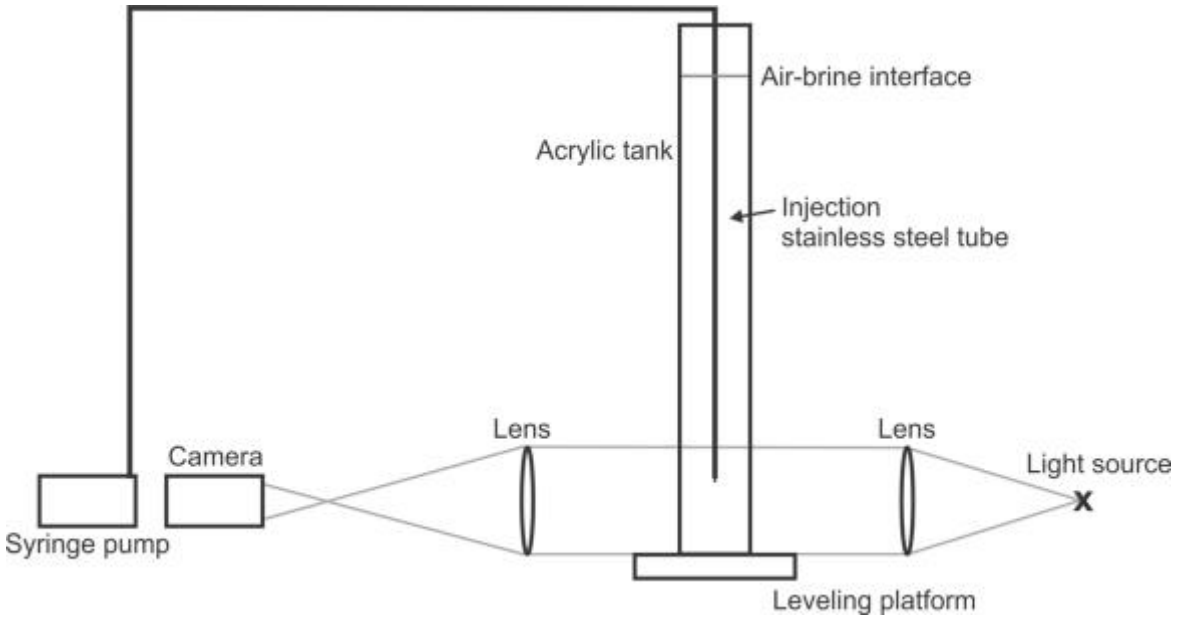

Figure 8. Schematic of the experimental setup for shadowgraph imaging at the base of the tank. Note that for imaging of the air-brine interface, the tank was lowered into the light path.

an initial transient) the tank base plate (Figure 9B) or impinge on the base plate and spread laterally up to some separation distance that is governed by buoyancy (Figure 9C). Figure 9D-F show results of thresholding grayscale images to create binary (black and white) images. Image processing was used to determine the injection depth, the location of the bottom of the tank, and the distance between the bottom of the tank and the injection depth, as shown in Figure 9D-F. Automated image processing measured the horizontal jet and return plume width. While the tank was leveled, the camera may not have been leveled exactly the same, thus images may seem askew. The width was thus measured in the perpendicular direction to the gray dashed lines of Figure 9D-F. For the 15 combinations of injection depth and flowrate, image processing was performed from the start of injection until the approximate time that: 1) circulation of downward moving mixed water enter the field of view at the height of the nozzle (see Figure 10A); or 2) the lateral spreading of the plume near the tank base touches the walls of the tank (Figure 10B–C). Figure 11 presents examples of plume widths as a function of injection depth, injection flowrate, and time for non-impinging and impinging cases (such data were collected for all 15 injection depth and flowrate pairs). Each vertical line represents a processed frame. Figure 11A shows that the plume for the flowrate and injection depth of 52.5 ml/min and 7.77 cm (~ 3 in), respectively, never touches the bottom of the tank—the maximum penetration depth is visible from the figure. The features of the downward moving non-impinging jet and upward rising plume are captured by Figure 11A. Figure 11B displays an example of an injection jet that propagates downward and impinges and spreads against the bottom of the tank for essentially the entire test. The lighter gray values represent the width of the initial downward propagating jet, whereas the overprinting darker values represent the width of the rising buoyant plume that is detached from the bottom of the tank.

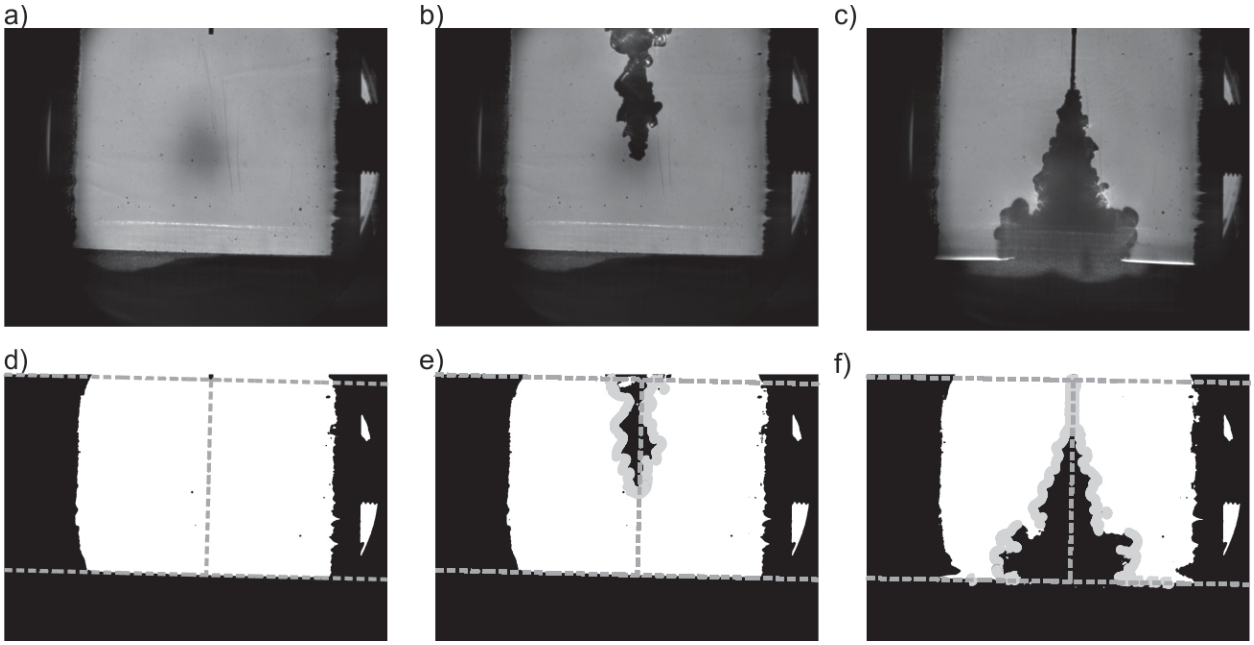

Figure 9. Original and processed shadowgraph images. A) Shadowgraph image of base of tank containing brine prior to injection of deionized distilled water. The injection nozzle is visible at the top center at a height of 7.62 cm. B) Shadowgraph image of injected water at a flowrate of 52.5 ml/min (3.20 in3/min), which penetrates into the brine column and never impinges against the base plate. C) Shadowgraph image of injected water at flowrate of 157.5 ml/min (9.61 in3/min), which impinges and spreads against the base plate. D, E, and F) Thresholded versions of Figures 9A, B and C. Dash lines were calculated by custom image processing algorithms, which determine the location of the base plate and the normal line between the nozzle and the base plate. The gray circles in Parts E and F highlight the margins of the plumes that were identified by the image processing algorithms.

Figure 12 presents the time-averaged width of the plume, between the injection depth and bottom of the tank, for all non-impinging cases (cases where the plume does not touch the bottom of the tank or only briefly at very early time; see Figure 9B, 9E, 10A, and 11A for examples of non-impingement). We define the plume to include the upward moving buoyant water in addition to the downward moving injected and entrained water (but we do not include the relatively downward moving mixture as seen at the top of Figure 10A).

Out of the 15 cases, lower flowrates and greater distances between the injection depth result in non-impingement, as expected. The case of 7.62 cm (3 in) injection depth and 105 ml/min exhibits the maximum rising plume and mixing near the injection depth. The plume width and penetration depth depend strongly on the jet flow rate—the key finding is that return plume width thus has a relation with *Re*. Control of the width of the return plume and the thus the depth of completely-mixed conditions for SPR applications can be affected by something that operations can readily adjust, the flowrate. The slopes of the right portions of the curves of Figure 12 indicate the growth of the rising plumes as they travel upward into the tank. The continued growth by the time the plumes reach the upper ABI is of interest to verify completely-mixed conditions at the ABI—imaging at intermediate depths with these techniques has not been conducted yet to verify the behavior and growth of the rising plumes. Intermediate-depth

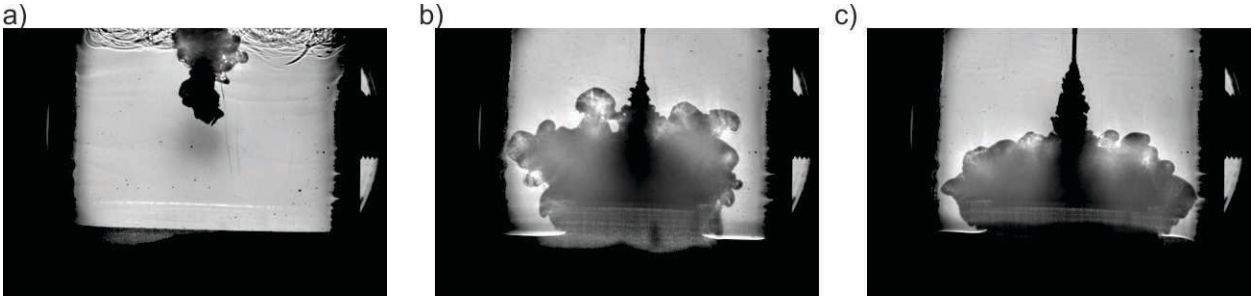

Figure 10. Representative mixing behaviors of the flow imaging experiments at the base of the tank for injection depth of 7.62 cm (3.0 cm; from the base of the tank), at the approximate time image processing is stopped. a) The injected water of flowrate 52.5 ml/min (3.20 in^3/min) and entrained plume is clearly visible in the middle as a dark region, surrounded at the top by relatively slow downward moving mixed water. From same data set as Figure 9b. b) The injected water of flowrate 157.5 ml/min (9.61 in^3/min) and entrained plume and buoyant plume are clearly visible. The rising plume touches the wall at the left. c) The injected water of flowrate 210 ml/min (3.20 in^3/min) at the time its rising buoyant plume first touches the side walls.

imaging could be part of future work to help define plume behavior such as where and when the return plume contacts the walls of a cavern. Such a study may help improve control of where leaching occurs in a cavern.

Figure 13 presents the plume widths, spatially averaged over a 0.25 cm (0.10 in) vertical zone near the bottom of the tank for the cases of jet impingement (see Figures 9C, 9F, 10B, and 10C for examples of jets impinging on the bottom of the tank). For the greater distance between the bottom of the tank and the injection depth (7.62 cm or 3 in), the plume width increases with time until the plume begins interacting with the walls of the vessel; the curves exhibit a decreasing-in-magnitude but still positive slope with time. For the 5.08 cm (2 in) injection depth, the higher flowrates of 210 and 158 ml/min exhibit change in (positive) slopes at later times; however, the 105 ml/min case shows a rise then slight drop to negative slopes with time. The 2.54 cm (1 in) injection depth cases show positive slopes that essentially become level at later times. These curves reach a steady-state plume width at the base; the progression of sizes is systematic with the lower flowrates having smaller steady-state basal plume widths. Thus, if greater mixing is desired for SPR, higher flowrates with basal impingement could be applied. Noise in the data of Figure 13 is due to image processing artifacts. Figure 14 presents the time-averaged (skipping over initial transients) and spatial-averaged (from injection depth to bottom of the tank) plume width for all 15 cases as a function of the jet *Re*. A key finding is that the plume width is linear with *Re* for a given injection depth up until impingement with the vessel base plate. Relating to SPR, the width of the return plume, and when it contacts the walls of the caverns, may thus be controlled by changing *Re* or the flowrate.

Top-of-tank imaging results for injection depths of 7.62 cm (3 inch) above the base of the tank show rising, well-mixed plumes for relatively low flowrates (1, 5, and 21 ml/min; see Figure 15A-C). We assume higher flowrates will also be well-mixed. Figure 15D-F is the only case that shows the development of a low-salinity bank of stratified water at the top of the tank—this is the case where the injection depth is near the air-brine interface and the flowrate is 1.0 ml/min.

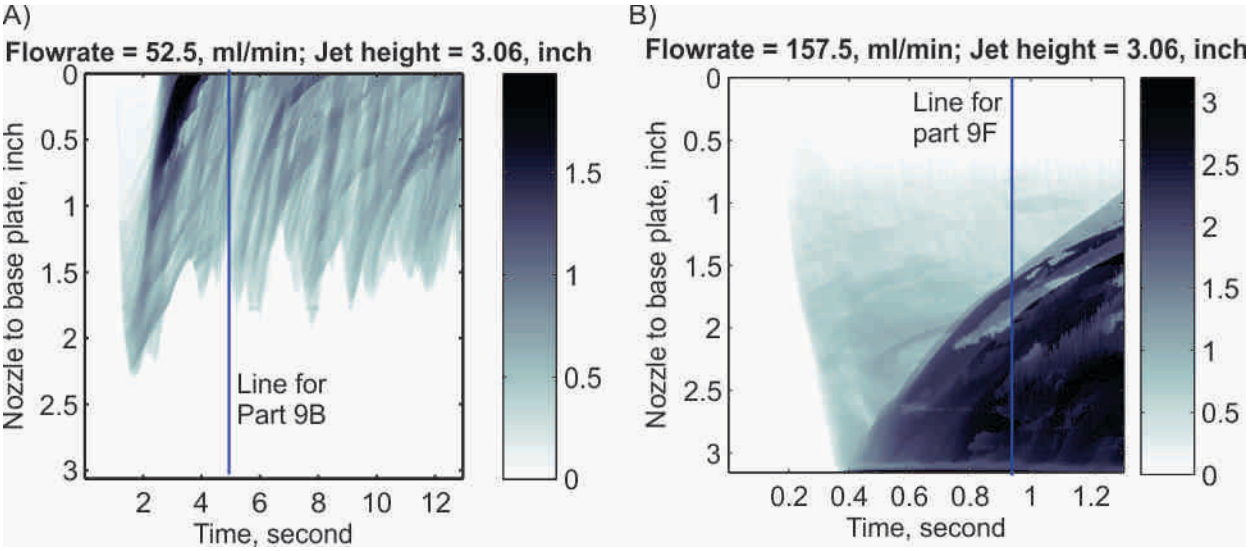

Figure 11. Plume width as a function of the distance between the injection depth and the tank base plate and time. The grayscale colorbar indicates the width of the plumes in inches normal to the centerline that connects the injection depth (nozzle) to the base plate (lines shown in Figures 9E and F). The vertical lines indicate the time at which the image frames for Figures 9E-F were taken.

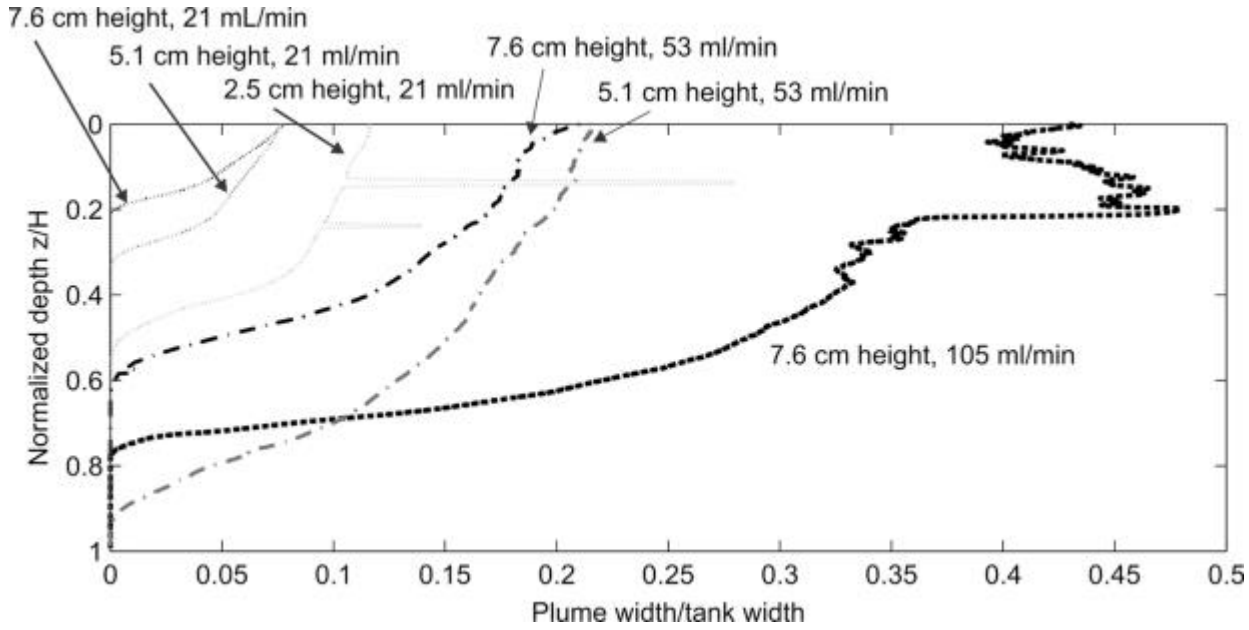

Figure 12. Time-averaged steady-state plume width normalized by tank width versus the distance z from the nozzle towards the base plate normalized by total injection depth-to-base-plate distance H. The locations where the curves touch the y axis thus represent the maximum relative (from injection depth to base plate) downward penetration distance of the fluid jet. The locations where the curves touch the (upper) x axis represent the maximum width of the rising plume at the depth of injection. Flowrates plotted include 21, 52.5, and 105 ml/min (or 1.28, 3.20, or 6.41 cubic inches/min). The other flowrates from the 15 combinations of injection depth and flowrate pairs exhibit base-plate impingement.

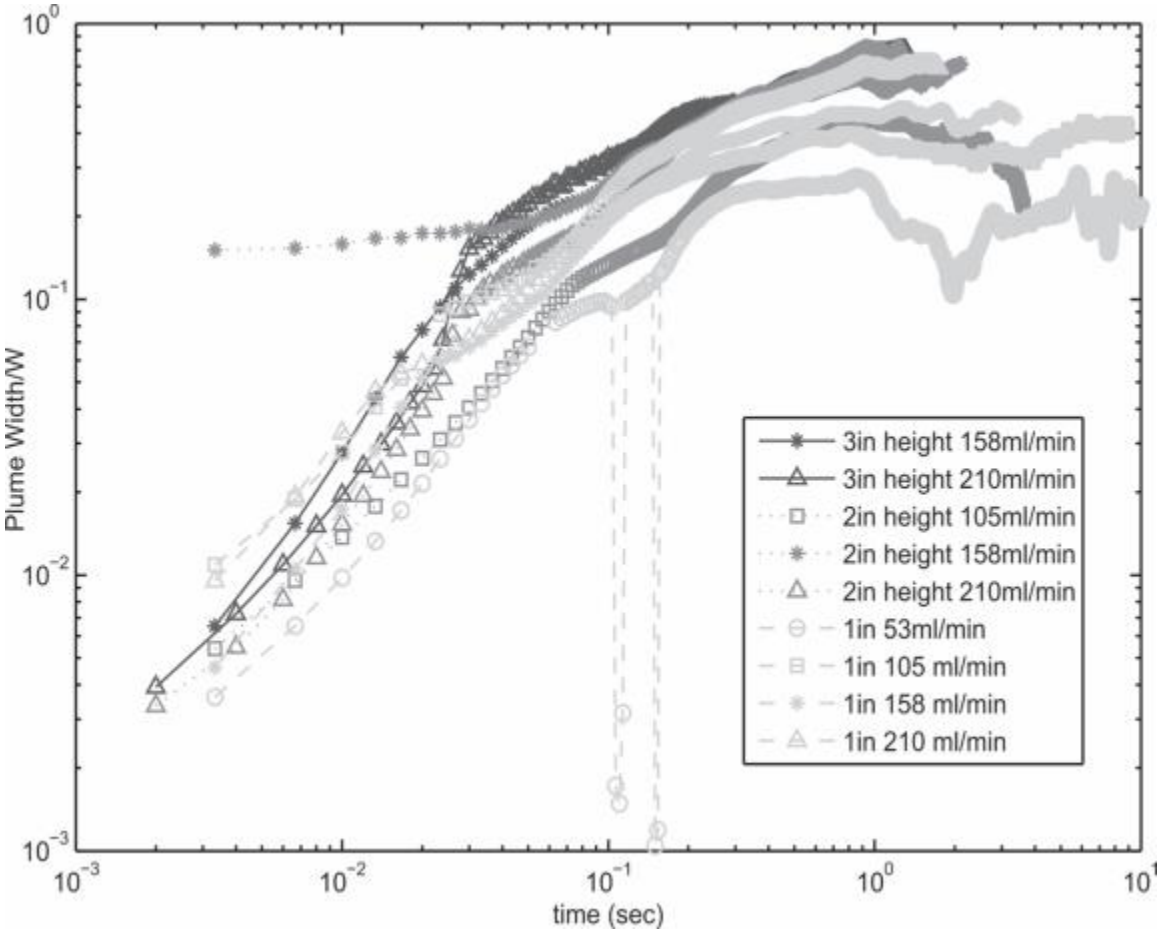

Figure 13. **Impinging plume width within ~ 0.25 cm (0.1 in) of the bottom of the tank (normalized by the tank width W) versus time (second).**

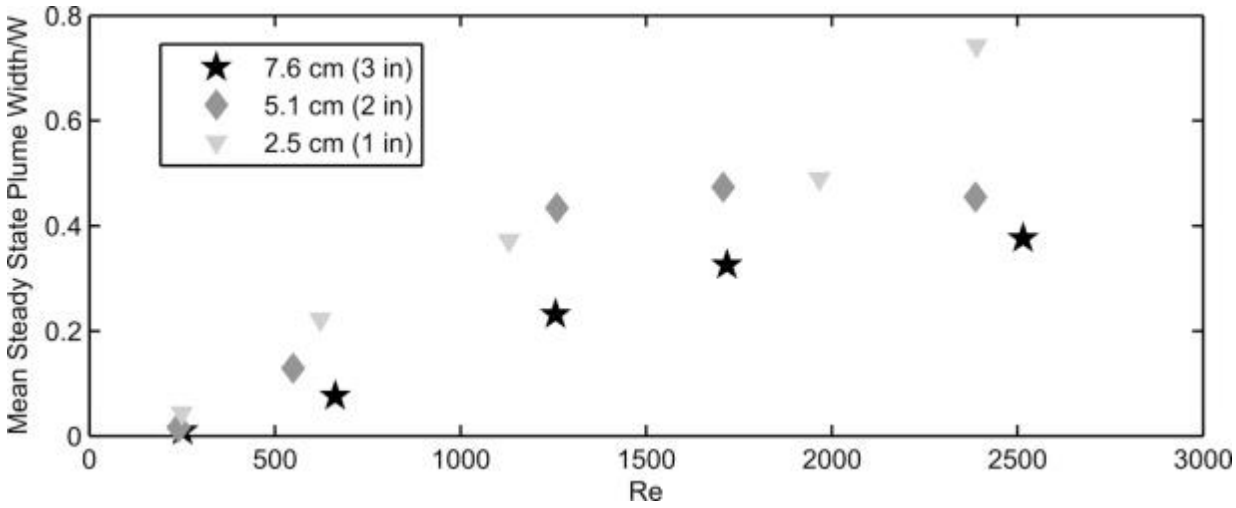

Figure 14. Time averaged and spatial-averaged plume width normalized by the vessel width as a function of *Re*. Notice that plume width is a strong (linear) function of the input momentum for the experiments at lower *Re*.

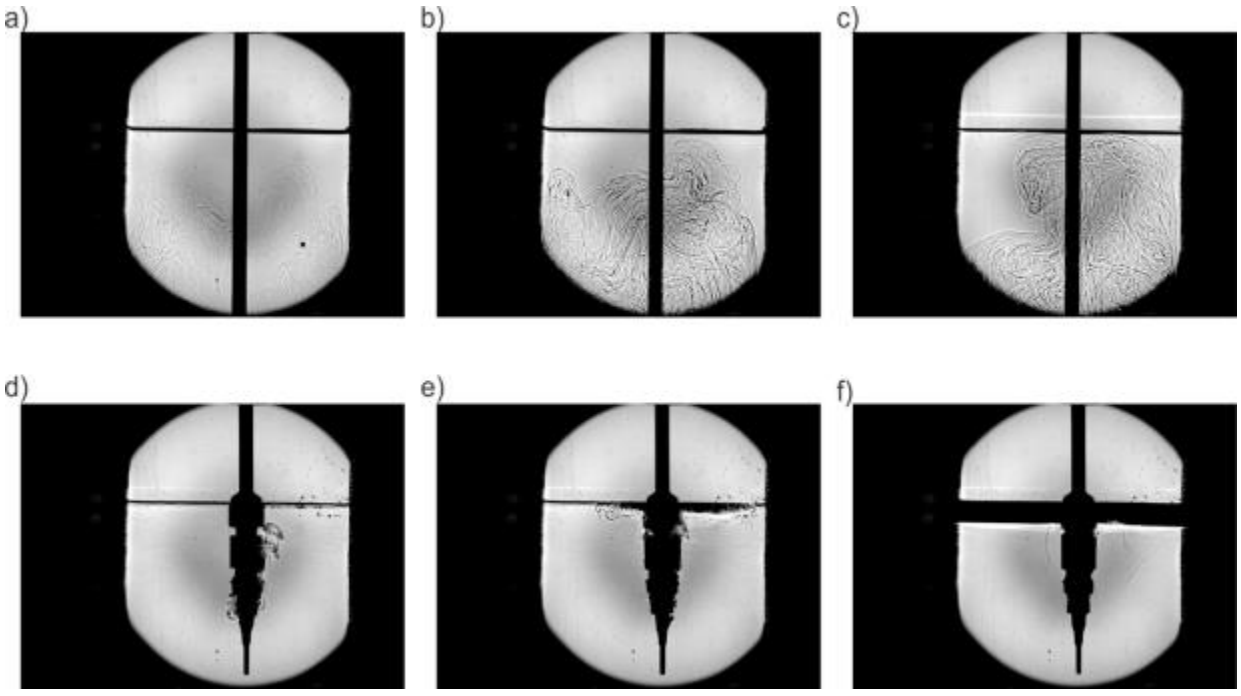

Figure 15. Imaging at air-brine interface near the top of the tank for injection depths at 7.62 cm (3 in) above base plate for Parts a-c, and ~5.08 cm (~2 in) below air-brine interface for Parts d-f. a) Flowrate of 1 ml/min and photo taken after 169.1 s of injection; diffuse plume nearly hits interface. b) Flowrate of 5 ml/min and photo taken after 55 s of injection immediately before plume near hits interface. c) Flowrate of 21 ml/min and photo taken after 38 s of injection and immediately after plume hits interface. d-f) Times series of the same experiment (at 0.5, 17.9 and 169 s) with nozzle near air-brine interface at flowrate of 1 ml/min, which is the only case showing a bank of poorly-mixed water building under the air-brine interface.

4.4. Upward Flow and Mixing of Injected Raw Water in Brine Near the Injection String

4.4.1. Introduction

In this Section 4.2 we present laboratory techniques using particle tracking methods to understand the physics of flow near the injection string and its influence on mixing of raw water and brine. As discussed in Section 4.1, imaging performed at the top of the tank at the air-brine interface (equivalent to the OBI) showed well-mixed conditions in the reservoir even for low flow rates with the injection depth near the base of the tank. Incomplete-mixing with formation of a stratified layer of fresh water was only observed when the injection nozzle was placed very close to the ABI and flowrates were low. Poorly-mixed water traveled, probably via boundary layer flow, up the nozzle and injection assembly to follow the fresh water layer. Thus, this section is an effort to further examine this potential mechanism for creating stratified raw water and brine. Abundant literature exists on laminar and turbulent boundary layers for flow along a flat surface or cylindrical object, including theory and quantification of the growth of the boundary layers (e.g., Jordan, 2014). However, specific literature on the buoyancy-driven, return-flow, boundary-layer dynamics along a cylindrical tube is sparse. Ahmad et al. (2015) only studied the return plume and its dilution from the initial penetration depth back to the location of the jet orifice and not further along the injection pipe. This Section focuses on scaled laboratory experiments designed to address this knowledge gap.

Based on the low flowrate findings of Section 4, a hypothesis is that the main impediment to mixing is the presence of a boundary layer of fresh water flowing upward along the brine string. The section investigates how the jet *Re* influences the boundary layer. The major research question is: does the presence of the injection string affect the degree of mixing and the formation of an upper bank of fresh or low-salinity water? Can the string act as an upward "flow guide" for the injected raw water? The goal is to understand the physics of flow near the string and its influence on mixing of injected water and brine and eventually apply the understanding gained to the field.

4.4.2. Methods

Experiments were performed in the 0.13 width-to-height aspect ratio acrylic rectangular prism tank (76.2 cm tall by 10.16 cm on a side square cross section; Figure 16) of Section 4.2. The inner diameter of the stainless steel injection pipe, without an injection nozzle, is 0.18 inch (0.46 cm)—giving a pipe diameter-to-cavern width of 0.045. Typical SPR caverns have an injection pipe to width diameter of 9.75 inch (0.248 m) over 70 m or 0.0035. Our current goal is to investigate the physics of the returning boundary layer flow along the injection pipe and the influences of these flow processes on forming an upper bank of fresh water—our goal is not to simply match the field conditions, but to first learn about flow along a tube. Deionized distilled water was injected through the injection pipe with a Harvard PHD-Ultra series syringe pump at varying flowrates from 0.2 to 80 ml/min at different depths of the pipe orifice below the air-brine interface. The air-brine interface was at 73.7 cm (29 inch or 1 inch from the top of the tank) from the bottom of the tank for all experiments. No oil was used in these experiments. Spherical lenses were used to focus light on the injection pipe (Figure 16B). Movies of the injection experiments

were made with a Phantom high speed camera (Figure 16B), typically with the room lights turned off. The injected water was seeded with grey polyethylene microspheres at 1.00 g/cm^3 with the size range of 27–45 μm (the buoyancy drag force on particles of this size should be negligible on the order of 1 μm/s (Guildenbecher, D., pers. commun., 2015). Camera settings and the light source were adjusted to provide images of the particles in the injected fluid. Particle tracking Matlab scripts from Blair and Dufresne (2008) were used to obtain particle tracks for the consecutive set of image frames. Matlab scripts were written to: threshold for the particles that were most in focus; apply the particle tracking scripts; calculate fluid velocities based on the particle tracks at locations of interest; and estimate return or boundary layer widths based on the location of the particle tracks (Figure 17). Velocity of the returning plume was measured in order to compare with existing literature on buoyancy-driven boundary-layer flows, whereas the boundary-layer flow examined herein is buoyancy driven but with the additional effect of initially downward directed jet momentum.

4.4.3. Results and Discussion

Figure 18 illustrates the quantification of the particle tracks and flow velocities of a representative flow experiment. Variance in the flow velocities are probably due to outlying values that were calculated from the full width of the return plume or boundary layer at a given depth (Figure 18). The return plume width, above the pipe orifice appears to thin; however, the intensity of light diminishes with height for this image setup and thus the thinning may also be an experimental artifact. Typically, boundary layers would be expected to grow in thickness. The obtained velocity profile transitions from lower values near the pipe orifice to higher values farther up from the pipe. A qualitative comparison of flows at the pipe orifice for flowrates of 2, 20, 50, and 80 ml/min and a depth of 39.1 cm (15.4 inch) below the air-brine interface shows an increase in the return plume thickness with flowrate (Figure 19). The plume appears to be attached to the pipe wall for flowrates up to 50 ml/min. At 80 ml/min, the plume appears turbulent and it is difficult to observe whether any of the upward moving fluid is attached to the pipe. The flows at 50 ml/min or less exhibit a constant penetration depth after initial transients dissipate.

Imaging of the pipe above the orifice and with a pipe orifice depth below the ABI of 40.0 cm (16.1 inch or approximately four injection opening diameters higher than Figures 4A–D) shows instabilities or waves developing on the boundary layer at a flowrate of 5 ml/min and smooth flow at a higher flowrate of 40 ml/min (Figure 19). Images of the pipe with a pipe orifice depth of 55.1 cm (21.7 inch or approximately 35 injection opening diameters higher than Figure 19A–D) do not show a boundary layer: the flow appears well-mixed as particles rise and disperse through the field of view (Figure 19G–H). Figure 20 compares the boundary layer or return plume velocities as a function of depth below the air-brine interface for a constant pipe-orifice depth and injection velocity. The comparison shows that the return plume velocity varies as a function of the injection velocity. The corresponding width of the return plume varies strongly as a function of the jet velocity.

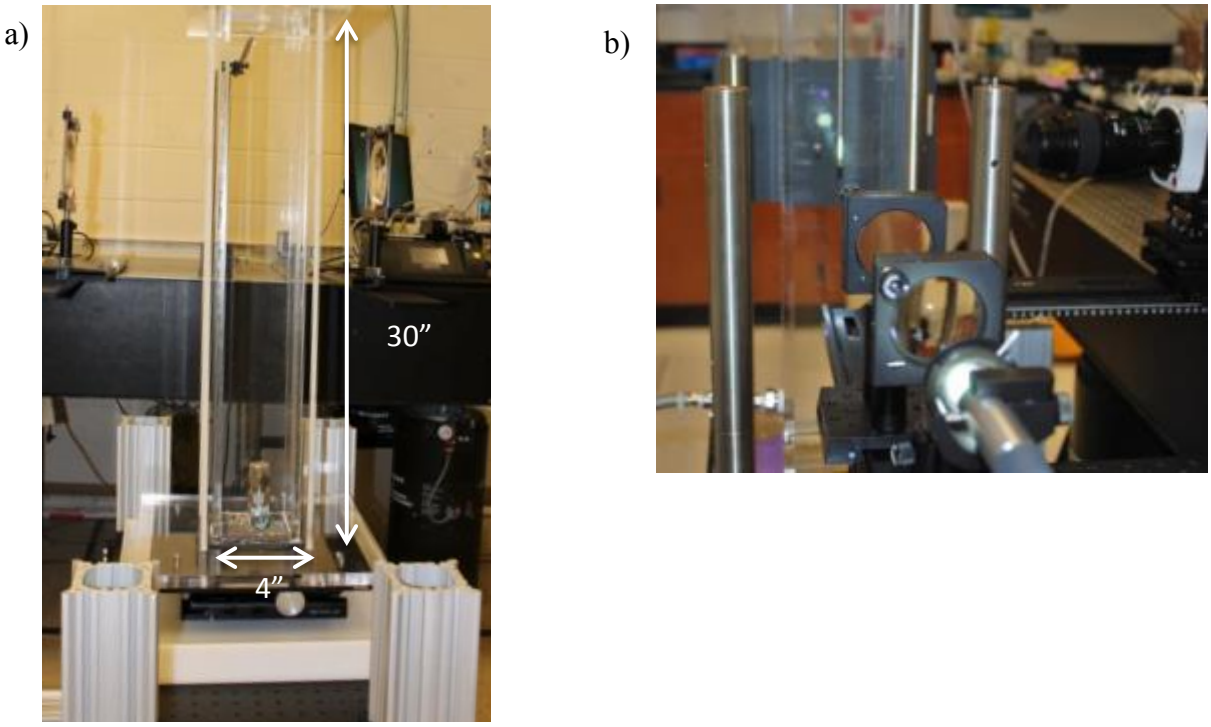

Figure 16. Photographs of A) the acrylic tank and B) the light source, the injection tube in the path of the light, the lenses used to focus the light, and the high speed camera on the right.

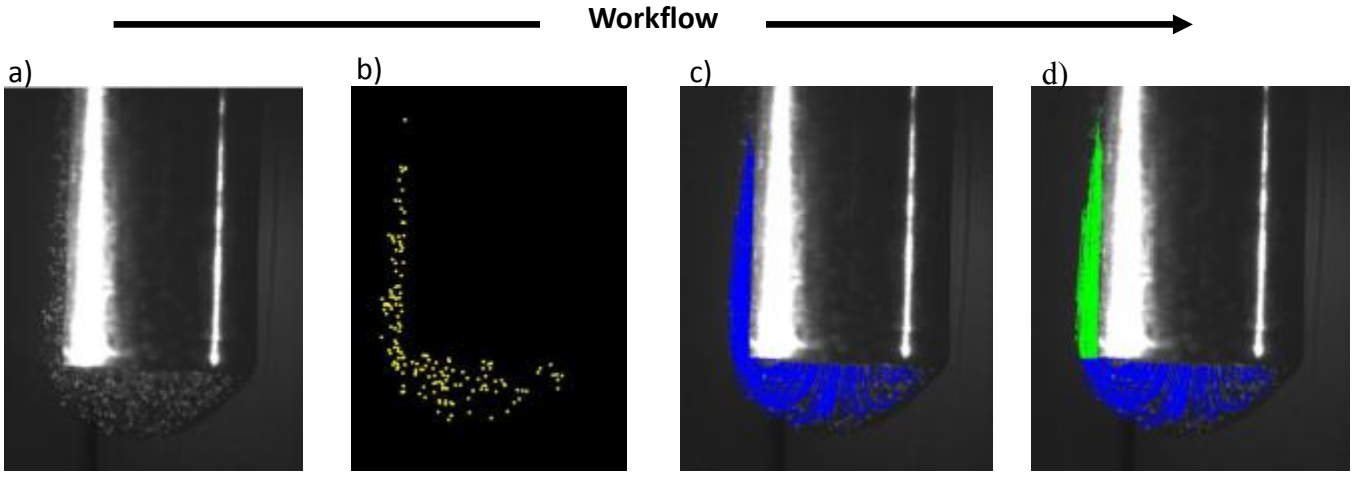

Figure 17. Images illustrating the imaging and postprocessing workflow, involving: A) an original image frame; B) segmentation for highlighting the particles with particle identification for one single frame; C) particle tracks for a given set of consecutive frames; and D) identification of particle tracks of interest for analysis (e.g., of velocity or flow width) using Matlab scripts.

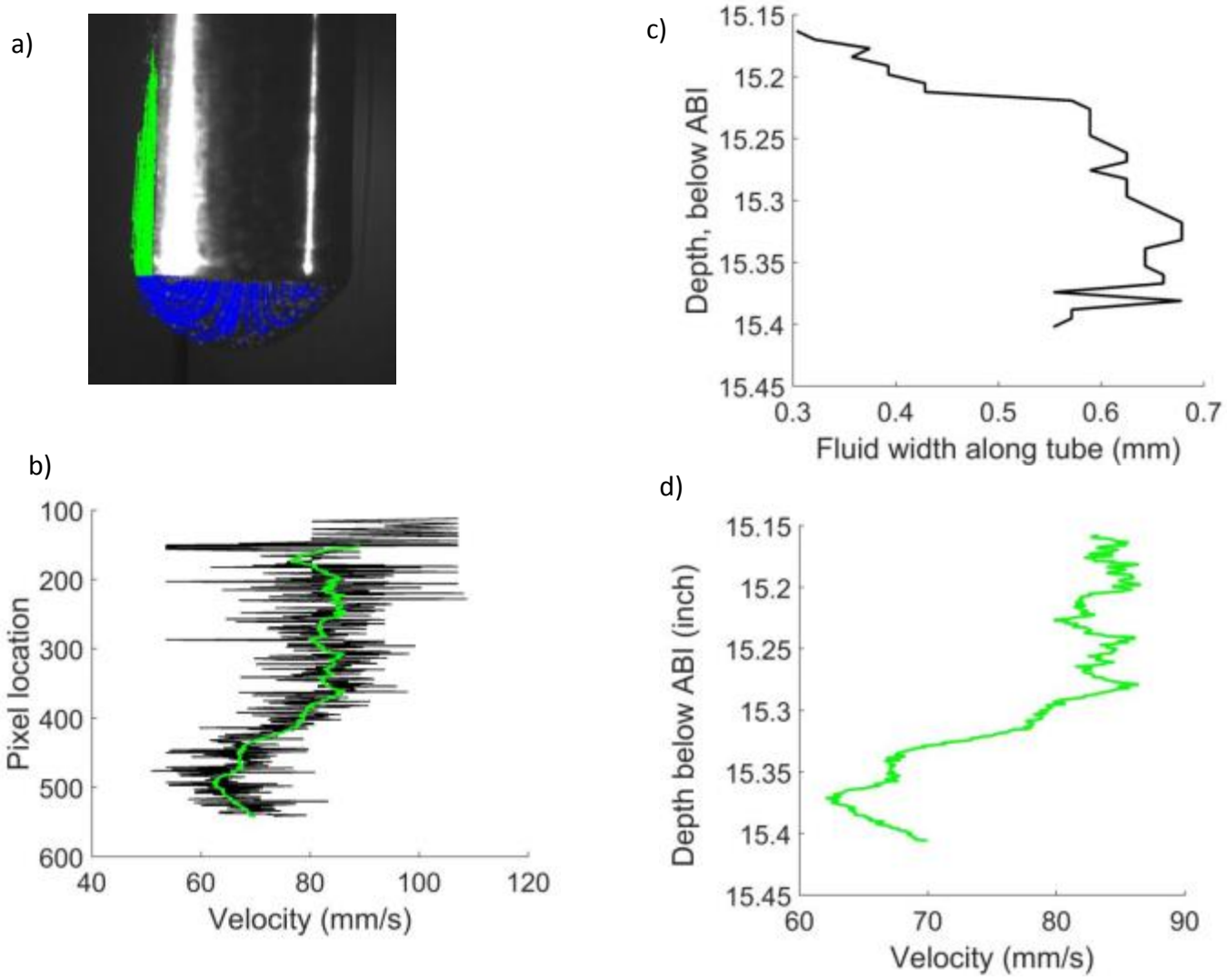

Figure 18. A) Particle tracks for a set of images. B) The calculated raw and moving-averaged particle velocity at a given vertical position (above the pipe orifice, shown in green in part a for all particles at a given vertical position. C) The width of the return plume or boundary layer versus depth below the air-brine interface (ABI). D) The moving-averaged fluid velocity from part b with depth below ABI (neglecting the upper data of part b).

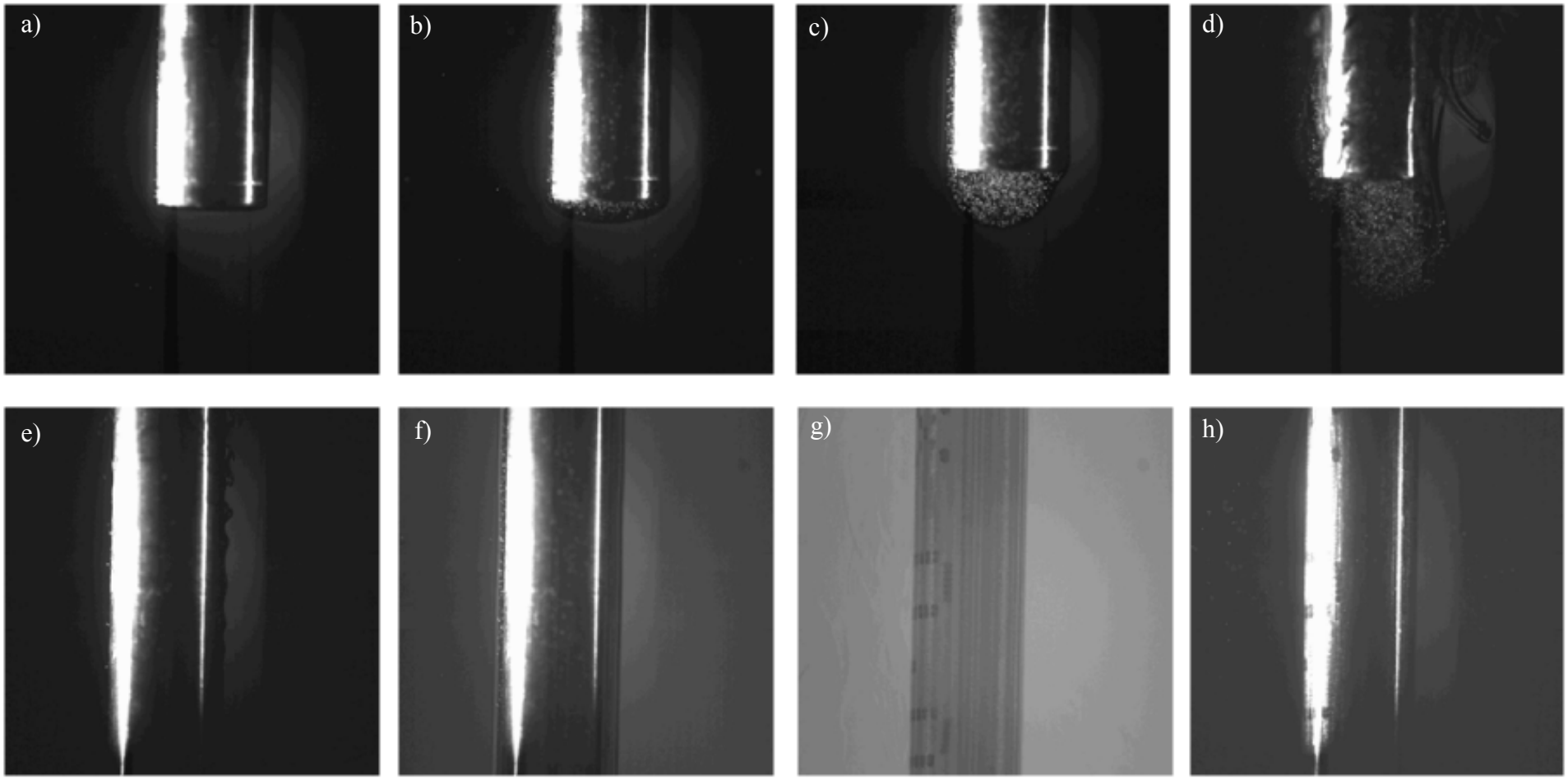

Figure 19. Particle tracking flow visualization images at the following depths of the tube orifice below the air-brine interface and flowrates: A) 15.4 inch, 2 ml/min; B) 15.4 inch, 20 ml/min; C) 15.4 inch, 50 ml/min; D) 15.4 inch, 80 ml/min; E) 16.1 inch, 5 ml/min; F) 16.1 inch, 40 ml/min; G) 21.7 inch, 2 ml/min; and H) 21.7 inch, 40 ml/min. Image G was taken with the room lights on.

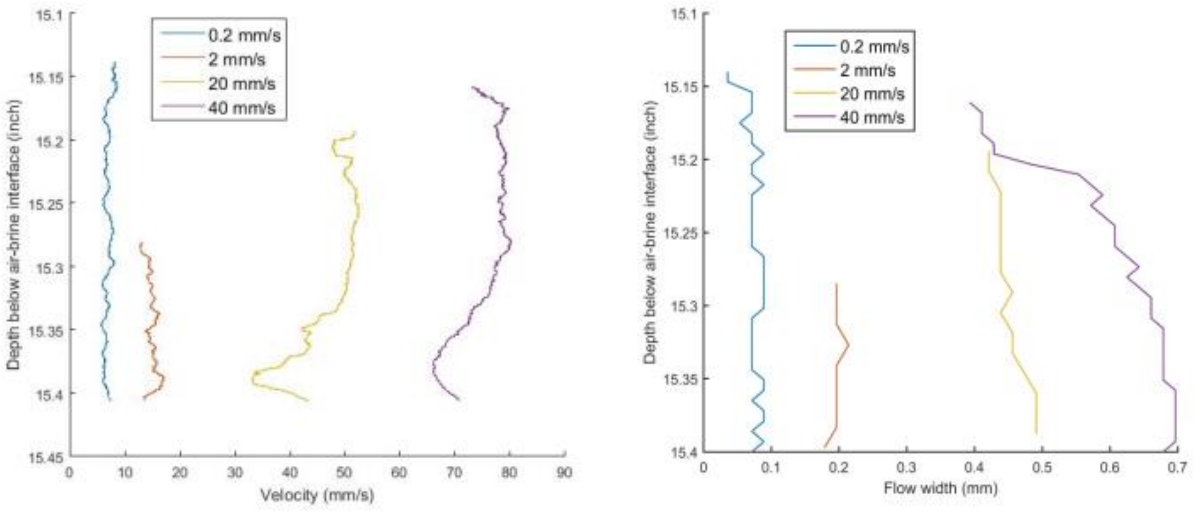

Figure 20. a) Averaged velocity of return plume (boundary layer) and b) width of return plume versus depth from air-brine interface for the four jet flow velocities: 0.2, 2, 20, and 40 mm/s.

The obtained boundary-layer velocity profile, which transitions from lower values near the pipe orifice to higher values further up the pipe, is qualitatively consistent with a boundary layer driven by buoyancy. Acceleration occurs due to the buoyancy driving force acting on the lower-density fresh water.

The boundary-layer velocity and boundary-layer width grow with increasing injection velocity. This occurs because the width of the boundary-layer increases with increasing injection velocity, which reduces the drag on the boundary layer due to the presence of the pipe (i.e., the highest drag occurs at the no-slip interface, assuming some degree of parabolic flow in the boundary layer). Thus, one would expect that in an experiment in which little-to-no initial momentum is imparted to the boundary layer, but the boundary-layer thickness is varied, that the boundary-layer velocity would also increase with increased initial boundary-layer thickness (again due to the decreased drag). Thus, the initial momentum of the jet may not remain in the boundary-layer fluid, and certainly must vanish at some point along the pipe, but influences the momentum of that fluid by altering the boundary-layer width.

To understand how these results may influence the field scale, we derive some quantitative estimates for the boundary layer properties by assuming that classical boundary layer theory adequately describes a boundary layer formed around the string in an SPR cavern. If the boundary layer is laminar, meaning that viscous forces contribute non-trivially to the flow behavior, and non-buoyantly, then we can expect the thickness of the boundary layer, δ, to grow according to $\delta = 5*Re^{-1/2}$ (Bernard and Wallace, 2002). The Reynolds number of the flow, Re, is defined here as $Re=Ud/\nu$, where U is the mean velocity of the flow at the location of the string exit plane, d is the string diameter, and ν is the kinematic viscosity of the raw water. If the

boundary layer is turbulent, meaning that inertial forces dominate the fluid dynamics, and non-buoyant then we expect $\delta = 0.382 * Re^{-1/5}$ (Bernard and Wallace, 2002).

The growth of the laminar and turbulent boundary layers is plotted in Figure 21 for SPR flowrates. Injection rates can vary from 20,000 to 100,000 bbl/day in typical SPR operations, resulting in an exit plane velocity ~ 1–10 m/s. Typical string diameters are on the order of 10's of cm. The kinematic viscosity of water at 20°C is 1.00×10^{-6} $m^2 s^{-1}$. Thus, we expect typical SPR operations to involve injection *Re* on the order of 10^5-10^6. These Reynolds numbers generally indicate turbulent rather than laminar flow. The resultant boundary layer thickness grows with depth according to Figure 21. To bound the flow behavior, we also use lower *Re* values of 10^3-10^4 to calculate thicknesses of a laminar boundary layer. At 100 m from the string outlet, the boundary layer ranges from 2.4 m thick for turbulent flow with a $Re = 10^6$ to 16.0 m thick for a laminar flow with a $Re = 10^3$. The location at which the boundary layer thickness reaches the wall of the cavern may provide an estimate of the bottom location for a bank of water, assuming there were no other processes working to mix the fluid. The boundary layer never reaches the wall in the turbulent case, further supporting a completely-mixed cavern. In the laminar case, the boundary layer reaches the wall at ~300 m from the injection depth for the lowest flowrate $Re = 10^3$, suggesting a 700-m deep pool. For $Re = 10^4$, the boundary layer reaches the wall at the cavern roof, suggesting only a thin pool would form. However, other processes, such as boundary layer separation, are highly likely for such flow rates according to our results and would tend to mix the water and brine long before it reached the cavern wall. The mixing decreases both the likelihood for a raw water pool to form and the depth of the pool if formed.

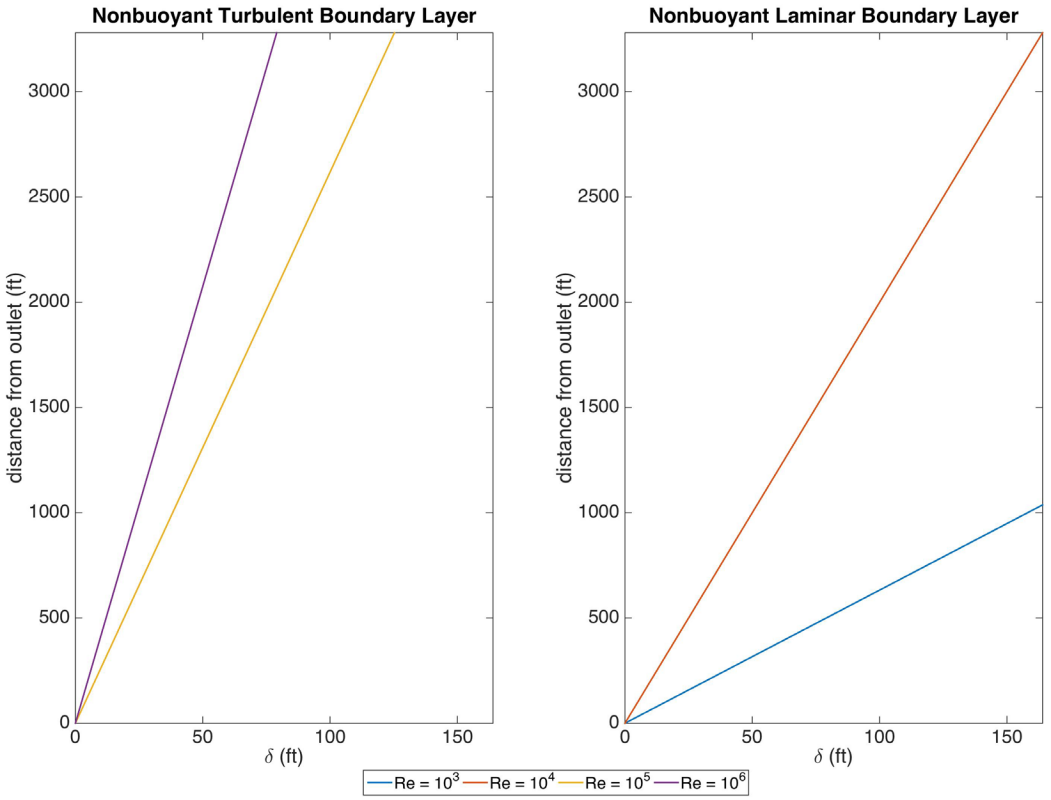

Figure 21. Estimates for (left) turbulent and (right) laminar boundary layer widths a range of injection flowrates.

5. SUMMARY

Regular field leaching and oil drawdown operations of SPR in tall and cylindrical caverns have been accurately modeled with assumptions of complete mixing between injected raw water and brine (see Section 3.2). In contrast, some experimental studies presented evidence of poor mixing and non-uniform dissolution, with cavern shapes that flared upward or had an undercut at the OBI. Our recent laboratory studies (Section 4), support the likelihood of complete mixing during standard flowrate ($Re \sim 10^6$) leaching operations in SPR caverns with tall and cylindrical shapes. For both of the new factors we considered, injection depths close to the cavern floor and a wide range of injection rates, we expect complete mixing. When the injection is near the floor, we expect the raw water jet to collide with and spread along the cavern floor contributing to a high degree of mixing with the brine. For a range of flowrates, flow of unmixed or poorly mixed raw water (the return plume) near the vicinity of the injection pipe will still tend towards complete mixing as the return plume is boundary-layer like and will separate and efficiently mix at a distance of several pipe diameters from the injection depth. Only short travel distances and low flowrates will create a bank of fresh water under the OBI, based on our findings. Normal SPR operations are unlikely to generate these conditions. Future field studies should document the range of flowrates, especially on the low end to determine the probability of low rates, which may increase the probability of poor mixing.

6. REFERENCES

Ahmad, N., and Baddour, R.E., 2015, Density effects on dilution and height of vertical fountains. Journal of Hydraulic Engineering 141, 04015024.

Bernard, P.S., and Wallace, J.M., 2002, Turbulent flow: analysis, measurement, and prediction: Hoboken, New Jersey, Wiley, 512 p.

Dimotakis, P.E., 2000, The mixing transition in turbulent flows: Journal of Fluid Mechanics 409, 69-98.

Eyermann, T. J., 1984, Comparison of SANSMIC Simulation Results with Cavern Shapes on the SPR Project, SMRI Spring Meeting 1984: Atlanta, Georgia, Solution Mining Research Institute.

Khalil, I., and Webb, S. W., 2006, Numerical Simulations of Lab-Scale Brine-Water Mixing Experiments: Sandia National Laboratories, SAND2006-5418, 138 p.

Lord, D. L., Roberts, B. L., Gutierrez, K. A., and Rudeen, D. K., 2012, Solution Mining Characteristics of US Strategic Petroleum Reserve Oil Drawdown, SMRI Spring 2012 Conference: Regina, Saskatchewan, Canada, Solution Mining Research Institute, 13 p.

Nath, C., Voropayev, S.I., Lord, D., Fernando, H.J.S., 2014. Offset turbulent jets in low-aspect ratio cavities. Journal of Fluids Engineering 136, DOI: 10.1115/1.4026023.

O'Hern, T., Hartenberger, J. D., and Webb, S. W., 2010, SPR salt wall leaching experiments in lab-scale vessel - Data report, SAND2010-7584: Sandia National Laboratories, 58 p.

O'Hern, T.J., Webb, S.W., Ehgartner, B.L., 2004. "Experimental Plan for Leaching Plume Studies in Lab-Scale Vessel." Sandia National Laboratories memo, November 12, 2004.

O'Hern, T.J., 2005. "Leaching Plume Studies in Lab-Scale Vessel - Experimental Analysis Completed." Sandia National Laboratories memo, October 24, 2005.

O'Hern, T.J., Oelfke, J.B., and Webb, S.W., 2005. "Preliminary Results of and Analysis Plan for Leaching Plume Studies in Lab-Scale Vessel." Sandia National Laboratories memo, February 28, 2005.

O'Hern, T.J., and Oelfke, J.B., 2005. "Leaching Plume Studies in Lab-Scale Vessel - Experiments Completed." Sandia National Laboratories memo, August 4, 2005.

Philippe, P., Raufaste, C., Kurowski, P., Petitjeans, P., 2005, Penetration of a negatively buoyant jet in a miscible liquid, Physics of Fluids 17, 053601.

Russo, A. J., 1981, A Solution Mining Code for Studying Axisymmetric Salt Cavern Formation, SAND81-1231, 33 p.

-, 1983, A User's Manual for the Salt Solution Mining Code, SANSMIC: Sandia National Laboratories, SAND83-1150, 44 p.

Reda, D. C., and Russo, A. J., 1983, Experimental Studies of Oil Withdrawal from Salt Cavities via Fresh-Water Injection: Sandia National Laboratories, SAND83-0347, 51 p.

-, 1984, Experimental Studies of Salt Cavity Leaching via Fresh-Water Injection: Sandia National Laboratories, SAND84-0020, 32 p.

Voropayev, S.I., Nath, C., Fernano., H.J.S., 2012, Mixing by turbulent buoyant jets in slender containers, Physics Letters A 376, p. 3213–3218.

Warren, J.K., 2016, Solution mining and salt cavern usage, *in* Warren J.K., ed., Evaporites: A Geological Compendium, Springer International Publishing, Switzerland, p. 1303-1374.

Webb, S.W., in review, Summary of externally-driven cavern oil mixing research at SNL including work performed at ASU/Notre Dame and UMass-Dartmouth: SAND report.

Webb, S. W., Lord, D. L., and O'Hern, T. J., 2011, Leaching Model Summary: Sandia National Laboratories, FY11-2.4(a1), 47 p.

Weber, P. D., 2015, SANSMIC Design Document, SAND2015-6334, 68 p.

Weber, P. D., Gutierrez, K. A., Lord, D. L., and Rudeen, D. K., 2013, Analysis of SPR Salt Cavern Remedial Leach Program 2013, SAND2013-7078, 62 p.

Weber, P. D., Rudeen, D. K., and Lord, D. L., 2014, SANSMIC Validation, SAND2014-16980, 106 p.

DISTRIBUTION

External Distribution

Electronic copies to:

Wayne Elias (wayne.elias@hq.doe.gov) for distribution to DOE SPR Program Office, Washington, DC

Diane Willard (diane.willard@spr.doe.gov) for distribution to DOE and FFPO SPR Project Management Office, New Orleans, LA

Sandia Distribution

Electronic copies to:

MS0899 Technical Library. 9536


Sandia National Laboratories